© 2018. Published by The Company of Biologists Ltd | Development (2018) 145, dev173187. doi:10.1242/dev.173187

CORRECTION

Correction: Divergent early mesoderm specification underlies distinct head and trunk muscle programmes in vertebrates (doi: 10.1242/dev.160945)

Nitya Nandkishore, Bhakti Vyas, Alok Javali, Subho Ghosh and Ramkumar Sambasivan

There was an error in the supplementary data of *Development* (2018) **145**, dev160945 (doi: 10.1242/dev.160945).

Two panels in Fig. S1 were reproduced from the supplementary material (Fig. S4) of an earlier paper, *Development* (2017) **144**, 4522-4529 (doi: 10.1242/dev.153262).

The panels in Fig. S1 have been replaced. The images in both cases show the same genotype but, for one panel, at a slightly different stage (E10 as opposed to E10.5). The updated file is now available online at http://dev.biologists.org/content/145/18/dev160945.supplemental.

This error does not affect the conclusions of the paper. The authors apologise to readers for this mistake.

© 2018. Published by The Company of Biologists Ltd | Development (2018) 145, dev160945. doi:10.1242/dev.160945

Divergent early mesoderm specification underlies distinct head and trunk muscle programmes in vertebrates

Nitya Nandkishore[1,2,*], Bhakti Vyas[1,3,*], Alok Javali[1,4], Subho Ghosh[1] and Ramkumar Sambasivan[1,‡]

ABSTRACT

Head and trunk muscles have discrete embryological origins and are governed by distinct regulatory programmes. Whereas the developmental route of trunk muscles from mesoderm is well studied, that of head muscles is ill defined. Here, we show that, unlike the myogenic trunk paraxial mesoderm, head mesoderm development is independent of the T/Tbx6 network in mouse. We reveal that, in contrast to Wnt and FGF-driven trunk mesoderm, dual inhibition of Wnt/β-catenin and Nodal specifies head mesoderm. Remarkably, the progenitors derived from embryonic stem cells by dual inhibition efficiently differentiate into cardiac and skeletal muscle cells. This twin potential is the defining feature of cardiopharyngeal mesoderm: the head subtype giving rise to heart and branchiomeric head muscles. Therefore, our findings provide compelling evidence that dual inhibition specifies head mesoderm and unravel the mechanism that diversifies head and trunk muscle programmes during early mesoderm fate commitment. Significantly, this is the first report of directed differentiation of pluripotent stem cells, without transgenes, into progenitors with muscle/heart dual potential. Ability to generate branchiomeric muscle *in vitro* could catalyse efforts in modelling myopathies that selectively involve head muscles.

KEY WORDS: Head muscles, Cranial mesoderm, Cardiopharyngeal mesoderm, Skeletal muscle differentiation, Wnt inhibition, Tbx6

INTRODUCTION

In vertebrates, head muscles serve functions such as sensory perception (by moving the eyes), feeding (by opening and closing the jaw) and breathing, as well as vocal expression (by controlling the larynx). Their function is strikingly different from those of trunk muscles, which primarily aid in locomotion. Ontogenetically, trunk muscles develop from the segmented trunk paraxial mesoderm, i.e. somites, whereas head muscles derive from the unsegmented head/cranial mesoderm (Evans and Noden, 2006). The extraocular head muscle group derives from the premandibular head mesoderm subtype. The branchiomeric group, which develops from the pharyngeal arches, and includes jaw, laryngeal and facial muscles, shares a common pool of progenitors with the heart known as the cardiopharyngeal mesoderm (CPM; Diogo et al., 2015; Grifone and Kelly, 2007; Kelly et al., 2001, 2004; Lescroart et al., 2010, 2014, 2015; Stolfi et al., 2010; Tirosh-Finkel et al., 2006; Tzahor and Evans, 2011). The specialized head muscles, along with the chambered heart, are considered crucial for the behavioural transition from filter-feeding invertebrate ancestors to active predation among vertebrates (Diogo et al., 2015; Gans and Northcutt, 1983). Despite this enormous evolutionary importance, little is known about the early mechanisms governing specification of head mesoderm.

Molecular differences between the head and somitic trunk muscle programmes are well documented (Bothe and Dietrich, 2006; Buckingham, 2017; Hacker and Guthrie, 1998; Harel et al., 2009; Lu et al., 2002; Sambasivan et al., 2009, 2011; Tajbakhsh et al., 1997; Tzahor et al., 2003). However, the source of this divergence is obscure. Mutant mouse studies have revealed the central role of the feedback loop involving Wnt/β-catenin and FGF4/8 signals, as well as T (brachyury) and the Tbx6 T-box transcription factor network, in the specification of trunk paraxial mesoderm upstream of trunk muscles (Chapman and Papaioannou, 1998; Ciruna et al., 1997; Deng et al., 1997; Galceran et al., 1999; Herrmann, 1991; Naiche et al., 2011; Yamaguchi et al., 1999). However, the early mesoderm specification programme of premandibular mesoderm and CPM is unclear.

Mesoderm emerges from the primitive streak at the posterior pole of the embryo, induced by the concerted action of BMP4, Nodal (TGFβ), Wnt/β-catenin and FGF signals along with *T* (Arnold and Robertson, 2009; Ramkumar and Anderson, 2011). The late-streak population develops at the posterior pole, where sustained Wnt/β-catenin and FGF4/8 signals induce *Tbx6* to specify trunk paraxial mesoderm (Arnold and Robertson, 2009; Aulehla and Pourquie, 2010; Martin and Kimelman, 2012; Mendjan et al., 2014; Ramkumar and Anderson, 2011; Turner et al., 2014). However, mesoderm from the early streak migrates to the anterior pole (Lawson et al., 1991; Tam and Beddington, 1987), wherein it downregulates *T* and begins to express key regulators of heart and head muscle lineages, such as *Tbx1*, *Pitx2*, *Isl1*, *Nkx2.5*, *Tcf21* and *Msc* (Diogo et al., 2015; Kelly et al., 2004; Lu et al., 2002; Nathan et al., 2008; Sambasivan et al., 2009, 2011; Shih et al., 2008). The cues driving this developmental progression and, thus, specifying head mesoderm are unclear.

Our work reveals that the mechanism diversifying the head and trunk muscle pathways occurs at an early step in mesoderm fate commitment. Here, we show that the development of head mesoderm and head muscles is independent of *T* and *Tbx6*, unlike that of trunk paraxial mesoderm. Furthermore, in contrast to the Wnt and FGF-driven trunk pathway, we show that the CPM subtype of the head mesoderm is specified by Wnt/β-catenin and Nodal inhibitory cues of the embryonic anterior pole. Moreover, by simulating the developmental sequence specific for CPM development with external cues, we have generated progenitors with skeletal muscle and cardiac twin potential from pluripotent embryonic stem cells. Notably, by uncovering and recapitulating the

[1]Institute for Stem Cell Biology and Regenerative Medicine, GKVK Campus, Bellary Road, Bengaluru 560065, India. [2]SASTRA University, Thirumalaisamudram, Thanjavur 613401, India. [3]Manipal Academy of Higher Education, Manipal 576104, India. [4]National Centre for Biological Sciences, TIFR, GKVK Campus, Bellary Road, Bengaluru 560065, India.
*These authors contributed equally to this work

‡Author for correspondence (ramkumars@instem.res.in)

R.S., 0000-0001-8158-4367

Received 25 October 2017; Accepted 31 July 2018

Development (2018) 145, dev160945. doi:10.1242/dev.160945

ontogenetic trajectory, we have generated progenitors specific to branchiomeric muscles. This marks a significant advance towards modelling and treating diseases selectively involving head muscles.

RESULTS

Head muscle development is *T*/*Tbx6* independent

To dissect the specification of mesoderm that generates head muscles, we assessed the requirement of T/Tbx6 pathway, which is crucial for the somitic programme of trunk muscles. *T* is an early marker and is expressed in all mesoderm. However, *Tbx6* RNA is detected in the primitive streak around embryonic day E7 in mouse embryos (Fig. S1A; Chapman et al., 1996), suggesting induction at least in the late emerging subset of head mesoderm. Our lineage-tracing analysis using *Tbx6-Cre* mouse line and $Pax7^{GPL}$, a Cre-responsive tissue-specific reporter, showed robust reporter expression in all developing muscles in the embryo, including those in head (Fig. 1A). Consistently, analysis employing the ubiquitous *ROSA* reporter revealed expression in extraocular muscle progenitors derived from premandibular mesoderm, the core of pharyngeal arches, which generate branchiomeric muscles, and in heart (Fig. S1A-C). Thus, in addition to the documented expression in trunk paraxial mesoderm, our genetic tracing shows that the *Tbx6* locus is at least transcriptionally induced in all of mesoderm that generates head muscles.

Next, we addressed the functional requirement of *T* and *Tbx6* in muscle development from head mesoderm. *Tbx6* mutants carrying the muscle reporter $Myf5^{nlacZ}$ displayed no observable head muscle phenotype at E11.5 (Fig. 1B). Muscle anlage in the pharyngeal arches and in the extraocular region developed normally, as in heterozygote littermates. In stark contrast, somites below the forelimb were completely missing, whereas the cervical somites display mispatterned myotome (Fig. 1A; Chapman et al., 1996). The patterning of the forelimb muscle anlage and the tongue progenitors revealed that the migratory progenitors from cervical somites were unaffected (Fig. 1B). These results, supported by analyses of other marker transcripts such as *Myf5* and *Myod* (both muscle markers), *Twist1* (a mesoderm and head neural crest marker) and *Sox10* (a proxy marker for mesoderm development) (Fig. 1C, Fig. S2A,B) confirmed unaffected head muscle mesoderm in *Tbx6* mutants, as opposed to severe disruption in trunk. Analysis of head mesoderm in *T* null (T^{Wis}) mouse mutants using *Myf5* reporter also revealed unperturbed development of the pharyngeal arch muscle core (Fig. 1E, Fig. S2C). Thus, the individual knockouts revealed no apparent role for *T* and *Tbx6* in myogenesis from head mesoderm.

Tbx6:Myf5 mutants underscore head and trunk muscle divergence

The core myogenic programme includes the bHLH muscle regulatory factors Myf5 and Myod. Notably, the crucial requirement for *Pax3* and *Tbx1*, genes upstream of the core myogenic programme, has been revealed only in the *Myf5* mutant background (Sambasivan et al., 2009; Tajbakhsh et al., 1997). Therefore, as a rigorous test of *Tbx6* function, we analysed *Tbx6:Myf5* double mutant embryos and control littermates using the $Myf5^{nlacZ}$ reporter. Strikingly, X-gal staining showed unperturbed branchiomeric and extraocular muscle development (Fig. 2A). Although the extraocular muscle loss is reported in $Myf5^{nlacZ}$

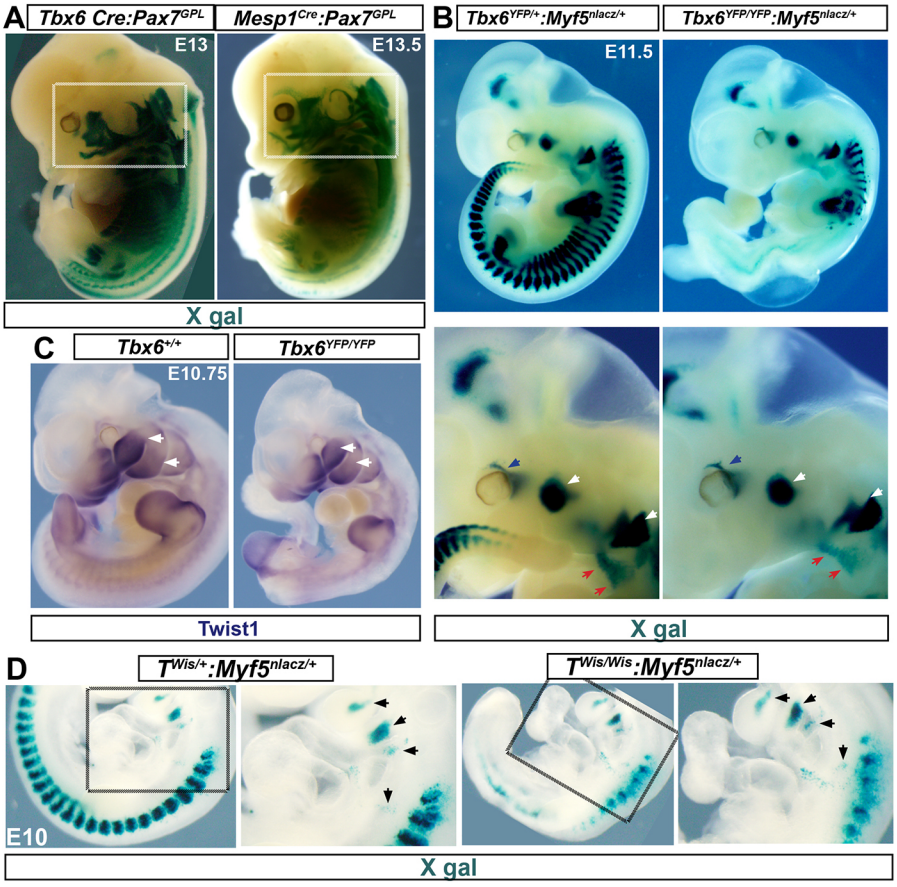

Fig. 1. Head mesoderm-derived muscle development unaffected by *T* or *Tbx6* loss of function, unlike that of somites. (A) Whole-mount X-gal staining shows *Tbx6* lineage tracing into head mesoderm-derived muscles. The *Tbx6-Cre* reporter marks the posterior neural tube, which is a neuromesoderm derivative (Javali et al., 2017). $Pax7^{GPL}$, a strong reporter, also reveals broader expression of $Mesp1^{Cre}$ than documented earlier (see Fig. S1A). Boxed area indicates the muscle derivatives of head mesoderm. (B) Whole-mount X-gal staining of littermates for $Myf5^{nlacZ}$ reporter. Blue arrows, developing extraocular muscles; white arrows, 1st and 2nd arch muscle progenitors; red arrows, migrating tongue progenitors. *n*>6 embryos. (C) Whole-mount RNA *in situ* hybridization of littermates. White arrows, expression in 1st and 2nd arches. (D) Whole-mount X-gal staining of littermates for Myf5nlacZ reporter. T^{wis} is a *T* (*Brachyury*) mutant allele. Black arrowheads, muscle progenitors in pharyngeal arches.

Development (2018) 145, dev160945. doi:10.1242/dev.160945

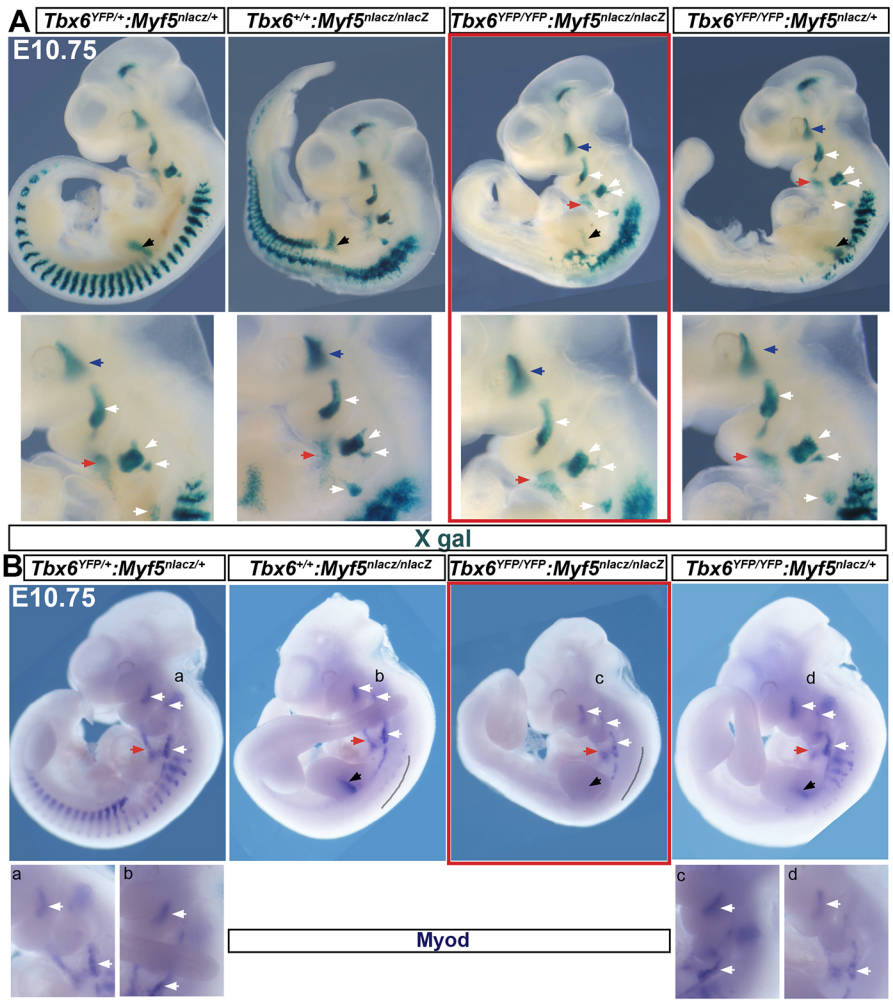

Fig. 2. *Tbx6:Myf5* mutant phenotype attests to *Tbx6*-independent head muscle mesoderm development. (A) Whole-mount X-gal staining of littermates for $Myf5^{nlacZ}$ reporter; *n*=4 double-null embryos. (B) RNA *in situ* hybridization for *Myod*. Deficiency in epaxial myotome (black line) appears to be additive. Accounting for minor differences in age among littermates, no obvious reduction in *Myod* signal is observed either in pharyngeal arches or in forelimb (black arrows; see Fig. S2). Blue arrows, developing extraocular muscles; white arrows, 1st, 2nd and posterior arch muscle progenitors; red arrows, migrating tongue progenitors. *n*=7 double-null mutants.

mutants, the phenotype is manifested only at a later stage (Sambasivan et al., 2009). Muscle progenitors from the cervical somites, which form the myotome, migratory tongue progenitors and forelimb muscle anlage displayed a phenotype similar to that of *Myf5* mutants. Because deficiency downstream of *Myf5* is possible, we analysed the progression in the myogenic lineage by *Myod* RNA *in situ* hybridization. *Myod* expression appeared unaffected in all of the six *Tbx6:Myf5* double mutants analysed, with no significant reduction in the pharyngeal arches or in the cervical somites (Fig. 2B, Fig. S2D). The absence of phenotype specifically in the 1st and 2nd arches was consistent with unaffected *Tbx1* expression, a key myogenic factor for jaw and facial muscles, in *Tbx6* mutants (Fig. S2E). The weaker forelimb signal with both the *Myf5* reporter and *Myod* RNA is likely due to an overall developmental delay in double mutants relative to littermates, because marker expression in age-matched comparisons at E11.5 were comparable (Fig. S2D). In summary, muscle development from head mesoderm and cervical somites was unaffected in the *Tbx6:Myf5* double knockouts. In essence, the analyses of mutants underscore a broad divergence in anterior head and neck versus posterior trunk muscles at an early stage in the mesoderm specification programme.

Disrupting Wnt inhibition perturbs head mesoderm development

Although there is a differential requirement for T/Tbx6, the progenitors of both neck and trunk somites experience sustained Wnt/β-catenin and FGF signalling, and T/Tbx6 expression in the posterior pole around the primitive streak. However, head mesoderm develops in the anterior end of the embryo, the signalling environment of which contrasts with the Wnt3A- and FGF4/8-secreting posterior domain. Instead, the anterior signalling centre secretes inhibitors of Wnt and Nodal, such as Dkk1, Cer1 and Lefty1 in order to establish the anterior pole of the embryonic body axis (Arkell and Tam, 2012; Lewis et al., 2008; Perea-gomez et al., 2002; Yamamoto et al., 2004). We hypothesized that Wnt and Nodal inhibitory cues instruct the distinct head mesoderm identity upstream of the divergent head muscle pathway. To address this, we first assessed whether the anterior polarity cues and head mesoderm development coincide spatiotemporally. In tune with the inhibition of Wnt signal, *Axin2-d2EGFP*, a faithful reporter of Wnt/β-catenin activity (Jho et al., 2002), was completely absent in the anterior domain in the head-fold stage mouse gastrulae (Fig. 3A). *Cer1*, which encodes a secreted inhibitor of Nodal is also expressed in this spatiotemporal domain (Fig. 3A; Biben et al., 1998). We found that the expression of head mesoderm markers *Tbx1* and *Pitx2* map on to the domain under the influence of the inhibitory cues of the anterior signalling centre (Fig. 3A,B).

Next, we addressed whether the anterior signalling center plays any role in CPM development *in vivo*. To achieve this, we employed mouse embryo *ex utero* culture. This technique is challenging. Therefore, we focused on Wnt inhibitory cues, as *Axin2-d2EGFP* mouse strain, a facile tool with which to assess modulation of the

Development (2018) 145, dev160945. doi:10.1242/dev.160945

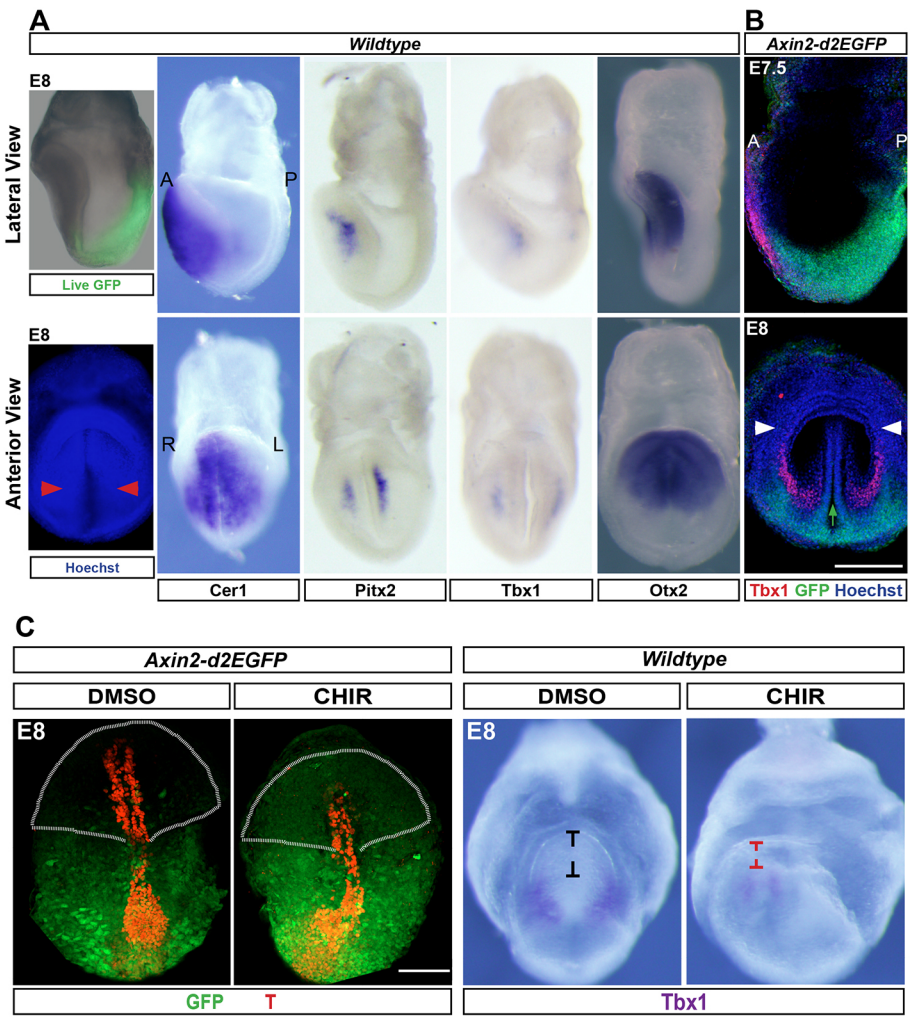

Fig. 3. Wnt-inhibitory cues spatiotemporally coincide with cardiopharyngeal mesoderm development. (A) Live GFP expression of Wnt-activity reporter Axin2-d2EGFP embryo superimposed on bright-field image. Right panels: *in situ* hybridization of stage-matched embryos show expression of head mesoderm markers. Cer1 is a multifunctional antagonist of the Nodal/BMP/Wnt pathways (Piccolo et al., 1999). Otx2 is a bona fide marker for the anterior pole (Ip et al., 2014). Anterior views of the same embryos are shown below in the bottom row. Hoechst-stained embryo is shown for anatomical reference, red arrowheads indicate head mesoderm. A, anterior; P, posterior; R, right; L, left. (B) Co-immunostaining of Axin2-d2EGFP embryos for Tbx1 and GFP shows mutually exclusive Tbx1 expression and Wnt activity. Green arrow, neural groove; white arrowheads, cardiac crescent. Images are representative of at least three embryos for each probe or staining. (C) Immunostaining shows ectopic induction of GFP in the Wnt-reporter embryos upon CHIR treatment. The yolk sac connecting the anterior and posterior halves has been ruptured to enable a frontal view of both the halves. Truncation of anterior domain is indicated by the outline, and black and red marks. RNA *in situ* hybridization reveals reduction in Tbx1 induction caused by masking Wnt inhibition. n=3 experiments and 6 embryos each for DMSO and CHIR treatment. Scale bars: 100 µm (B,C).

Wnt pathway, was available. Mouse embryos were collected at embryonic day (E) 7, at which point a significant proportion of head mesoderm progenitors have emigrated. In order to mask the anterior Wnt inhibitory cues, the embryos were cultured in the presence of a Wnt agonist (CHIR) for ∼24 h up to late head-fold stage and then phenotypically analysed. Embryos treated with CHIR showed expansion of the Wnt-reporter expression in *Axin2-d2EGFP* embryos to the anterior end of the embryo compared with vehicle control (DMSO; Fig. 3C). Even though the induction of the reporter is weak in the anterior end, the result revealed at least a partial masking of Wnt inhibition in the domain of head mesoderm development. We then analysed induction of Tbx1 as a measure of head mesoderm developmental progression in CHIR-treated wild-type embryos. Conspicuously, CHIR treatment resulted in truncation of the head region (Fig. 3C) reminiscent of the abrogation of the anterior signalling centre (Lewis et al., 2008; Thomas and Beddington, 1996). This serves as a phenotypic corroboration for the modulation of Wnt inhibition. Notably, we found substantially reduced *Tbx1* expression in CHIR-treated embryos (Fig. 3C). These findings suggest a role for Wnt inhibition in either the induction of *Tbx1* expression in head mesoderm or expansion/migration of head mesoderm. The technical limitation in the duration of *ex utero* embryo culture precluded the analysis of head myogenesis in these experiments. Nevertheless, our observations hint at a role for anterior polarity cues in head mesoderm development.

Wnt and Nodal dual inhibition confer cardiopharyngeal mesoderm identity

Our data indicate that the progenitors of head mesoderm are exposed to anterior polarity cues and that the cues may play a role in head mesoderm development. We addressed whether these cues confer head mesoderm identity to the nascent mesoderm population by employing a mouse embryonic stem cell (mESC) differentiation approach. Initially, embryoid bodies (EBs) were generated from mESCs and then exposed to the early streak signals BMP4 and the Nodal substitute activin A (‘mesoderm’; Fig. 4, Fig. S3A; Mendjan et al., 2014; Yang et al., 2008) for mesoderm induction. We obtained spheres of uniform size, which is key for efficient EB-mediated differentiation protocols (Fig. S3A; Behringer et al., 2016). This resulted in strong induction of *T*, *Tbx6* and other early streak markers (*Eomes*, *Gsc* and *Mesp1*), whereas *Tbx1* was not upregulated (Fig. 4B,C; Fig. S3B). Induction of *Sox17* and *Foxa2* (Fig. S3B) without upregulation of Sox2 indicated that the cells were nascent mesendoderm like, consistent with early streak identity. Subsequently, the EB-derived ‘mesoderm’ spheres were cultured with either the Wnt agonist CHIR 99021 and FGF2 (in place of FGF4/8) or with antagonists of Wnt (Dkk1 or Xav 939) and Nodal (SB431542). The former combination is reported to generate late streak mesoderm, the precursor of trunk muscle mesoderm (Mendjan et al., 2014); we refer to this as ‘posterior’ condition. The dual inhibition of Wnt and Nodal is the test that mimics cues from the anterior signalling centre. After 48 h of treatment, the cultures

Development (2018) 145, dev160945. doi:10.1242/dev.160945

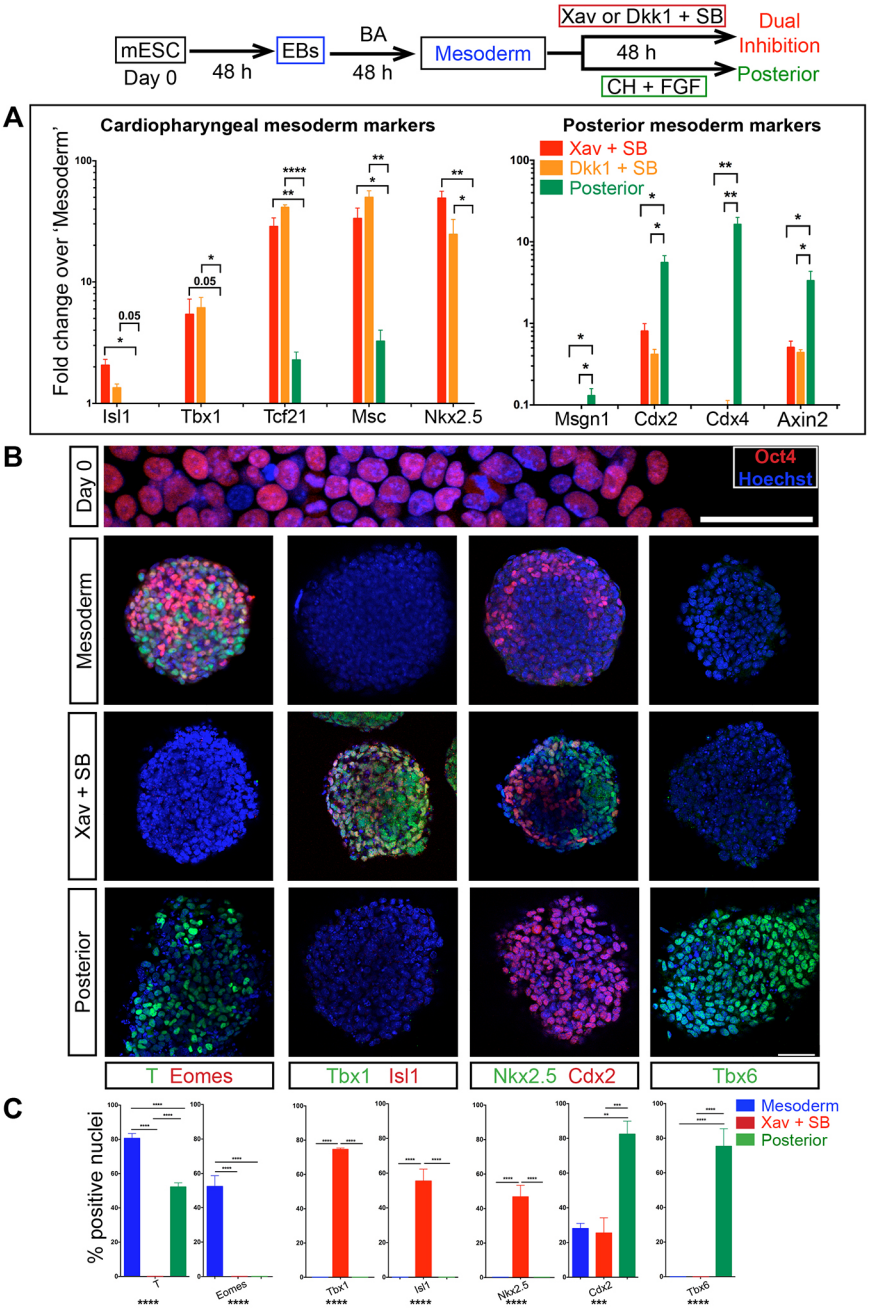

Fig. 4. Selective and robust induction of cardiopharyngeal mesoderm markers by anterior body axis polarity cues. Schematic outlines the regimen of treatments for differentiation. mESC, mouse embryonic stem cells; EBs, embryoid bodies; BA, BMP4 and activin A; Xav, Xav939 (Wnt inhibitor); Dkk1, Dickkopf-1 (Wnt inhibitor); SB, SB431524 (Nodal inhibitor); CH, CHIR 99021 (Wnt agonist); FGF, FGF2. (A) RT-qPCR analysis for marker genes comparing Xav+SB to 'posterior' and Dkk1+SB to 'posterior' reveals selective robust induction of key head mesoderm markers on dual inhibition. *n*=3 experiments. For all histograms, mean values from biological triplicates have been plotted; error bars are s.e.m.; *P* value is calculated using Student's *t*-test, unpaired, between Xav+SB or Dkk1+SB and 'posterior' is indicated above the bars. **P*<0.05, ***P*<0.01, *****P*<0.0001. (B) Immunostaining assay. Oct4 is a pluripotency marker. T/Bra and Eomes are mesoderm markers. Tbx1, Isl1 and Nkx2.5 are cardiopharyngeal mesoderm markers. Tbx6 and Cdx2 are posterior mesoderm markers. For split channels, see Fig. S3E. Scale bars: 50 µm. (C) Histograms show the proportion of marker-positive cells. T+ cells: 80.6±2.9% (mean±s.e.m.; total nuclei counted 543) in mesoderm, 52.3±2.3% (mean±s.e.m.; total nuclei 673) in posterior. Eomes+ cells: 52.5±6.2% (mean±s.e.m.; total nuclei 543) uniquely in mesoderm; Tbx1+ cells and Isl1+ cells: 74.6±0.8% (mean±s.e.m.; total nuclei 706) and 55.5±6.9% (mean±s.e.m.; total nuclei 1021), respectively, both uniquely in Xav+SB. Nkx2.5+ cells: 46.9±6.7% (mean±s.e.m.; total nuclei 992) uniquely in Xav+SB. Cdx2+ cells: 28.1±2.9% (mean±s.e.m.; total nuclei 815) in mesoderm, 25.5±8.8% (mean±s.e.m.; total nuclei 1428) in Xav+SB, 82.4±7.4% (mean±s.e.m.; total nuclei 581) in posterior. Tbx6+ cells: 75.4±10.1% (mean±s.e.m.; total nuclei 783) uniquely in posterior. *n*=3-5 experiments. For all histograms, mean values from biological triplicates have been plotted; error bars are s.e.m.; *P* value calculated by one-way ANOVA is indicated below the *x*-axis. Tukey's post hoc test was performed for multiple pairwise comparisons between differentiation conditions. The significance in *P* value by ANOVA is indicated below the *x*-axis and that of Tukey's above the bars. ***P*<0.01, ****P*<0.001, *****P*<0.0001.

were assayed by RT-qPCR. Reduced phospho-Smad2/3 levels confirmed Nodal inhibition by SB431542 (Fig. S4B). *Axin2* downregulation and reduction in total β-catenin levels verified effective Wnt inhibition by Xav as well as by Dkk1 (Fig. 4A, Fig. S4C). Remarkably, we found robust and selective induction of *Tbx1*, *Isl1* and *Nkx2.5*, as well as *Msc* and *Tcf21*, which are key cardiopharyngeal mesoderm (CPM)/branchiomeric muscle regulators (Lu et al., 2002) upon dual inhibition (Fig. 4A; for *Pitx2*, see Fig. S3F). In contrast, posterior markers such as *Cdx2*, *Cdx4* and *Msgn1* were upregulated or maintained in 'posterior', while suppressed upon dual inhibition (Fig. 4B). Immunostaining showed Tbx1, Isl1 and Nkx2.5 expression uniquely in dual inhibition (Fig. 4B,C; see Fig. S3D for low magnification and Fig. S3E for individual channels). On the other hand, uniform induction of Cdx2, initially induced in a small proportion of 'mesoderm' cells, and expression of Tbx6 protein is unique in the 'posterior' condition (Fig. 4B,C).

Pax3 is a key somitic muscle factor, which is neither expressed nor required in head mesoderm (Hacker and Guthrie, 1998; Tajbakhsh et al., 1997). Although *Pax3* RNA was detected in Xav+SB431542 (Fig. S3F), Pax3 protein was undetectable by immunostaining (not shown). We suspect that RNA of *Pax3*, which is also a neural marker, comes from the occasional Tbx1− Sox2+ neural progenitor clusters observed in dual inhibition cultures (Fig. S3F). In summary, based on selective induction of key markers upon dual inhibition, we conclude that Wnt and Nodal inhibitory cues specify CPM identity and possibly a pan-cranial mesoderm identity.

Our results show that inhibition of Wnt and Nodal confer CPM identity in a murine model. We tested whether these anterior

Development (2018) 145, dev160945. doi:10.1242/dev.160945

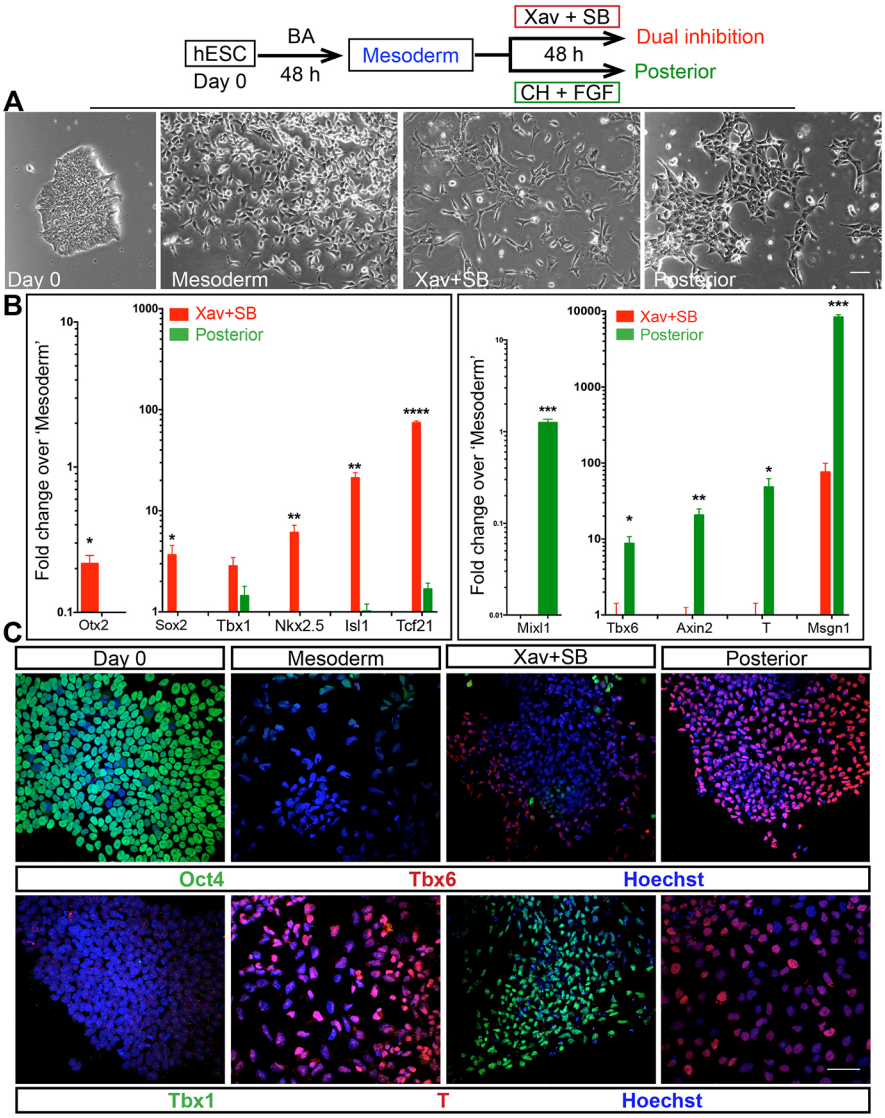

Fig. 5. Recapitulation of developmental cues guides human ESC differentiation into cardiopharyngeal mesoderm. Top panel outlines the experiment. (A) Micrographs taken during the course of differentiation. Cells in Xav+SB431542 appear more dispersed/migratory than in 'posterior'. (B) RT-qPCR analysis shows induction of CPM identity by dual inhibition in hESC. Mean values from three biological replicates; error bars are s.e.m.; Student's *t*-test, unpaired; **P*<0.05, ***P*<0.01, ****P*<0.001, *****P*<0.0001. (C) Immunostaining assay shows efficient induction of T in 'mesoderm' with a concomitant suppression of pluripotent marker Oct4 and mutually exclusive Tbx1 and Tbx6 expression in Xav+SB431542 and 'posterior', respectively. Scale bars: 50 µm (A,C).

polarity cues could guide similar differentiation of human embryonic stem cells (H9; hESCs; Fig. 5A). An RT-qPCR assay as well as immunostaining analyses revealed that the CPM markers were upregulated, whereas trunk mesoderm markers were repressed (Fig. 5B,C). These experiments also attest that the effect of anterior polarity cues is cell line-independent and suggests that this mechanism underlying head mesoderm/CPM identity is likely conserved across mammals.

Inhibition of Wnt and Nodal signals appears tightly coupled in CPM

We next tested whether inhibition of both Wnt and Nodal pathways was necessary or whether inhibition of either is sufficient. We compared Xav+SB431542 dual inhibition with treatments with either Xav alone or SB431542 alone. Treatment with inhibitors of either pathway individually resulted in significant and selective induction of the head mesoderm markers comparable with dual inhibition (Fig. S4A). Remarkably, the treatment with Xav alone resulted in significant reduction in pSmad2/3 levels (Fig. S4B). On the other hand, treatment with SB431542 alone led to a dramatic dip in total β-catenin levels (Fig. S3C). Thus, inhibition of either pathway appears to indirectly attenuate the other as well, suggesting that Nodal and Wnt pathways are tightly interconnected in early mesoderm. In fact, extensive crosstalk between Wnt/β-cat and Nodal-TGFβ pathways during development is known (Skromne and Stern, 2001; Guo and Wang, 2009) and Nodal induces Wnt to initiate gastrulation and mesoderm formation (Arnold and Robertson, 2009; Ramkumar and Anderson, 2011). In particular, TGFβ activates several Wnt ligands and elevates β-catenin levels (DiRenzo et al., 2016). Similarly, Wnt/β-catenin signal induces the expression of Nodal as well as its co-receptor Cripto (Morkel et al., 2003; Rodríguez-Esteban et al., 2001). In the context of CPM, the mechanism interlinking the inhibition of both the pathways remains to be explored.

Using the small molecules iCRT3 and iCRT5, which specifically inhibit β-catenin responsive transcription by blocking β-catenin – Tcf interaction (Gonsalves et al., 2011), we distinguished between the transcription function of β-catenin and its function in the cell membrane. The treatment with iCRTs also resulted in selective induction of most CPM markers assayed (Fig. S4A; iCRT3 data not shown). Thus, with regard to Wnt signal, inhibition of β-catenin-mediated transcription regulatory function may be key to induce CPM.

Development (2018) 145, dev160945. doi:10.1242/dev.160945

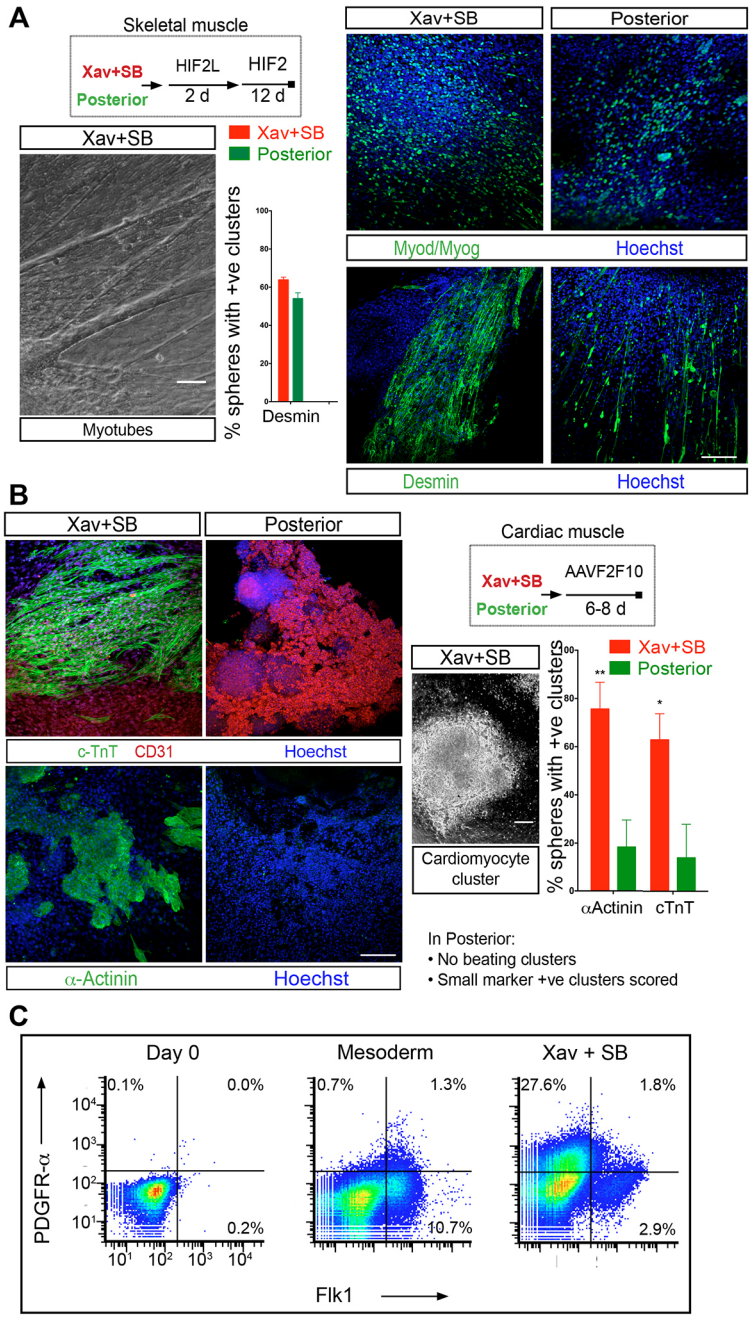

Fig. 6. Muscle and heart twin potential confirms cardiopharyngeal identity of dual inhibition-derived mesoderm. (A,B) Schematics of the experiments. H, HGF; I, IGF-1; F2, FGF2; L, LDN 193189 (BMP inhibitor); AA, ascorbic acid; V, VEGF; F10, FGF10. (A) Phase-contrast micrograph of bundles of myotubes following skeletal muscle differentiation of Xav+SB431542 culture by a method adapted from a previous report (Chal et al., 2015). Immunostaining for skeletal muscle markers Myod/Myog (antibodies specific to Myod and Myog combined) and desmin. Histogram shows the proportion of spheres associated with marker positive clusters of cells (see Materials and Methods). Xav+SB431542: desmin 63.9±1.4 (mean±s.e.m.); 'posterior': desmin 54.1±3.0 (mean±s.e.m.); n=3 experiments. Scale bar: 25 µm. (B) Micrograph of a cardiomyocyte cluster derived from Xav+SB431542. Immunostaining for cardiac markers cTnT, α-actinin and CD31 (an endothelial marker). Endothelial differentiation is consistent with the origin of vasculature in head from cranial mesoderm (Couly et al., 1992). Histogram shows the proportion of spheres associated with marker-positive clusters of cells. Xav+SB431542: α-actinin, 75.7±11.1%; cTnT, 62.8±10.8%. 'posterior': α-actinin, 18.4±11.2%; cTnT 13.9±13.9% (mean±s.e.m.). n=5 experiments. In Xav+SB431542, entire EB-derived spheres differentiated into beating cardiomyocyte clusters, whereas in 'posterior', a sphere was scored even if a small marker-positive cluster was associated with it. For all histograms, mean values from biological replicates have been plotted; error bars are s.e.m.; P values were calculated using Student's t-test, unpaired; *P<0.05 and **P<0.01. Scale bars: 100 µm. (C) Pseudo-colour scatterplot of flow cytometry analysis of PDGFR-α and Flk1 expression on day 0 (mESC) in mesoderm and Xav+SB431542-treated mesoderm. The figure is a representative of three experiments.

Dual inhibition-derived mesoderm has cardiac as well as myogenic potential

We have demonstrated that Wnt and Nodal inhibition impinge on the regulatory programme of CPM. To investigate further, we tested the potential of dual inhibition-derived cultures to differentiate into skeletal muscle and cardiomyocytes. This is a decisive test for CPM identity (Diogo et al., 2015; Grifone and Kelly, 2007; Tzahor and Evans, 2011). To achieve this, we treated dual inhibition-derived mesoderm with previously published muscle-induction regimen (Chal et al., 2015). Briefly, post dual inhibition, the cells were cultured for 2 days in media containing LDN193189 (LDN; a BMP inhibitor), HGF, FGF2 and IGF1. Subsequently, the cultures were maintained in the same growth factor cocktail minus LDN for 12 days. During this differentiation, cells in the culture began aligning and fusing with each other to differentiate into long multi-nucleated myotubes (Fig. 6A). Immunofluorescence for muscle markers Myod, Myog and desmin revealed large clusters of cells differentiating into skeletal muscle myotubes (Fig. 6A). This downstream skeletal muscle differentiation in Xav+SB431542-treated cultures is comparable with that of 'posterior' cells (Fig. 6A). Thus, the dual inhibition-specified mesoderm responds to myogenic cues to make skeletal muscle.

Next, we assessed the cardiogenic potential of Wnt- and Nodal-inhibited mesoderm. In fact, Wnt inhibition has been documented to be key in driving heart differentiation (Marvin et al., 2001; Schneider and Mercola, 2001; Yang et al., 2008). To address cardiogenic potential, dual inhibition cells were treated with ascorbic acid (AA) and VEGF (Cao et al., 2012; Kokkinopoulos et al., 2016; Takahashi et al., 2003), along with FGF2 and FGF10. The embryoid body-derived spheres differentiated readily and efficiently into beating

Development (2018) 145, dev160945. doi:10.1242/dev.160945

cardiomyocyte clusters, which expressed cardiac markers such as cardiac troponin T (cTnT) and α-actinin (Fig. 6B). In contrast, mesodermal cells from 'posterior' condition never generated beating cardiomyocyte clusters. A few cTnT/α-actinin positive clusters, very small compared with the dual-inhibition condition, were observed in 'posterior', which were scored as positive (Fig. 6B). Notably, in this 'cardiogenic' milieu, the dual-inhibition cultures also generated clusters of myotubes positive for Myod, Myog (Fig. S5A) and desmin (not shown). Together, these results attest to the twin cardiac/skeletal muscle potential of mesoderm treated with Xav+SB431542. Moreover, the twin potential conferred by dual inhibition is not cell line specific, as we have replicated the differentiation assay using a different mouse ES line (Fig. S5B).

As previously reported for a similar *in vitro* cell population, poor survival of the cells precluded clonal analysis (Chan et al., 2016; Swartz et al., 2016) and, thus, the test of bipotency in Xav+SB431542 culture. Instead, we assessed expression of PDGFRα and Flk1 to assess the proportion of cells that may contain bipotent cells. Flk1 is a marker of lateral plate mesoderm (Kataoka et al., 1997) and PDGFRα+Flk1+ cells represent cardiac fated population (Kattman et al., 2011), whereas a PDGFRα+ Flk1− subset may contain bipotent cells (Chan et al., 2016). We find that around 30% of the Xav+SB431542 cultures are PDGFRα+ Flk1−, and that uniquely Flk1+ and the double-positive subsets are minor (Fig. 6C). Although, these experiments do not provide direct evidence, they suggest that the dual inhibition-derived CPM-like population may contain bipotent cells. In summary, our data highlight the twin potential of Wnt and Nodal inhibited mesoderm, which attests to its identity as the progenitor of branchiomeric muscles.

DISCUSSION

Head muscles are functionally and ontogenetically distinct from somite-derived muscles and are a vertebrate novelty. Recent discovery that both branchiomeric head muscles and heart emerge from the unique 'cardiopharyngeal' developmental unit has triggered great interest in head muscle development and evolution. We reveal that head and trunk muscle programmes are inherently different by demonstrating that mesoderm patterning and specification by body axis polarity cues underlie the divergence (Fig. 7). This advance in understanding the development of head muscles offers insight into their evolutionary origin. Furthermore, we have uncovered the developmental cues specifying CPM with skeletal muscle/heart twin potential. This has allowed us to generate skeletal muscle of CPM lineage from pluripotent stem cells *in vitro*, which has the potential to enable efforts in modelling and treating muscular dystrophies differentially involving head muscles.

Emergence of specialized head muscles is key for the switch from filter feeding to active predation associated with vertebrate evolution (Gans and Northcutt, 1983). Whether this novel group arose from modification and elaboration of trunk programme or evolved independently is a key issue (Diogo et al., 2015; Onai et al., 2015; Sambasivan et al., 2011; Stolfi et al., 2010; Wachtler and Jacob, 1986). Our findings that Wnt inhibition confers CPM identity, upstream of the documented role in inducing branchiomeric myogenesis (Tzahor et al., 2003), indicates that Wnt inhibition is a recurrent theme in head muscles. This contrasts with the persistent role of Wnt/β-catenin pathway in the somitic muscle programme. In this context, the emergent theory that the opposing cues of Wnt have a deeply conserved role in establishing anterior-posterior body axis polarity (Niehrs, 2010; Petersen and Reddien, 2009) is significant. We suggest that CPM specification by Wnt inhibition, the conserved anterior polarity cue, reflects a deeper evolutionary origin of CPM and branchiomeric muscles independent of the Wnt-driven somitic programme.

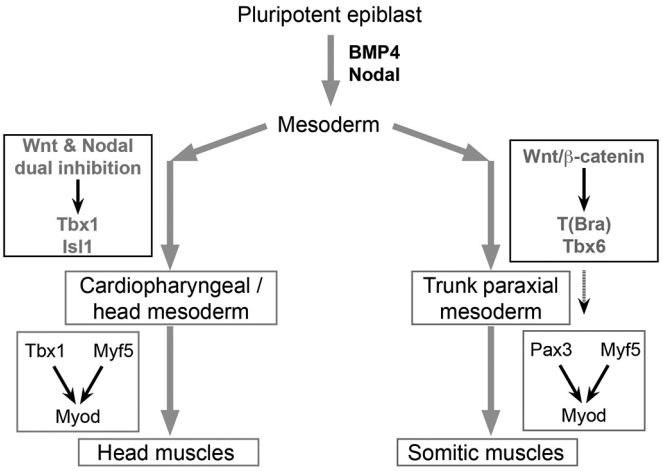

Fig. 7. Head and trunk muscle programmes are fundamentally divergent. A model based on our findings is illustrated. The Wnt, FGF and T network, induced by BMP4 and Nodal, triggers primitive streak and the formation of mesoderm at the posterior end of embryo. Trunk paraxial mesoderm, which forms somites, develops in the posterior pole of the embryo. It is specified by Wnt and FGF4/8 signals, which are sustained in the posterior pole. In contrast, head mesoderm progenitors migrate to the anterior pole and are specified by Wnt and Nodal dual inhibitors secreted in the anterior pole. Our study also reveals that the dual Wnt/Nodal inhibition-driven pathway is independent of T and Tbx6. This dichotomy in early mesoderm fate commitment lies upstream of head and trunk muscle divergence. Discovering how Wnt and/or Nodal inhibition impinge on the Tbx1/Pitx2/Isl1 network is the next challenge.

Differences in the transcription factor regulatory network of head and somitic myogenesis are well documented. Whereas the somitic muscles are *Pax3* driven (Tajbakhsh et al., 1997), head muscles are *Pax3* independent and are governed by *Tbx1*, *Isl1* and *Pitx2* (reviewed by Sambasivan et al., 2011). Our *Tbx6* and *T* mutant studies provide compelling evidence for the independence of the *Tbx1*/*Isl1* head regulatory programme from *T*/*Tbx6* mesodermal network. These findings point to either redundancy between *T* and *Tbx6* or to a pathway parallel to *T*/*Tbx6*, upstream of the head mesoderm programme. These possibilities remain to be addressed. In addition, dissecting the mechanistic link between Wnt and Nodal dual inhibition and the *Tbx1*/*Isl1* network is important to fully understand head muscle programme.

The early primitive streak signals BMP4 and Nodal pattern ESCs into mesoderm with cardiogenic potential (Mendjan et al., 2014). However, a variety of downstream cues, such as BMP2, retinoic acid and ascorbic acid in combination with VEGF and Wnt inhibition, have been employed for cardiac differentiation (Burridge et al., 2013; Keller, 2005). Whether these cues drive uniquely the cardiac lineage or broadly specify the bipotent CPM remained obscure. Investigating the inductive role for surrounding tissues on cardiac mesoderm in chick embryos, a pioneering study revealed that Wnt inhibition from anterior endoderm drives cardiogenesis (Marvin et al., 2001). Taking a similar approach to investigate the role of niche signals, we show that the body axis cues establishing anterior polarity, Wnt and Nodal antagonists, specify dual potential CPM. Remarkably, these antagonists are also secreted by anterior endoderm in mouse embryos (Stower and Srinivas, 2014). Taking these pieces of evidence together, we suggest that the BMP/Nodal primitive streak signals represent the early 'permissive' cue, whereas Wnt and Nodal dual inhibition at the anterior pole constitutes the 'instructive' cue that acts in tandem to progressively specify CPM. Unravelling

Development (2018) 145, dev160945. doi:10.1242/dev.160945

this developmental mechanism of CPM identity specification has allowed us to guide ESCs towards CPM-like progenitors with dual potential.

The ability to derive progenitors specific to muscle groups with distinct developmental history is pivotal to address disease mechanisms of muscular dystrophies. Directed ESC differentiation into skeletal muscle based on the trunk muscle programme has been reported only recently (Chal et al., 2015; Jiwlawat et al., 2018). To date, generation of cranial mesoderm-derived muscles from pluripotent cells has been elusive. Notably, forced expression of the bHLH factor Mesp1 programmes ESCs into cardiac/skeletal muscle bipotent CPM lineage (Chan et al., 2016). However, guided differentiation without transgene introduction is key for obtaining a regenerative cell type for therapy. Developmental signals specifying CPM identified here allowed us to simulate the developmental trajectory of the head muscle group. Such a strategy to recapitulate the ontogenetic programme appears crucial for efficient directed muscle differentiation (Chal et al., 2015) and may allow generation of progenitors specific to various muscle groups. We anticipate that our method will have a major impact by enabling generation of *in vitro* models of muscular dystrophies affecting head muscles as well as generating stem cells for therapy of dystrophies.

MATERIALS AND METHODS

Animals

Animals were handled according to Committee for the Purpose of Control And Supervision of Experiments on Animal (national) guidelines and the institutional animal ethics committee approved all animal experiments. Wild type refers to B6D2 (F1 of C57Bl/6J crossed to DBA/2) animals. Strains used are listed in Table S1.

X-gal staining

The embryos were fixed for 40 min to 1 h in 4% PFA, washed in PBS and stained overnight at room temperature in a standard X-gal staining solution.

In situ RNA hybridization

Whole-mount RNA *in situ* hybridization was performed following an established protocol (Henrique et al., 1995). The incubation period for proteinase K treatment was empirically determined for different stages of the mouse embryos. The antisense riboprobes were generated by *in vitro* transcription incorporated with digoxigenin-11_UTP (Roche). Washes following the incubation with alkaline phosphatase (AP)-conjugated anti-digoxigenin-11 antibodies were extended for 48 h and BM Purple (Roche) was used as the substrate for AP. For reliable comparison of *in situ* hybridization signals between mutants and control littermates or age-matched controls, each set of embryos was hybridized in the same tube. In the case of *ex utero* cultures, the vehicle-treated and CHIR 99021-treated embryos were hybridized in different tubes, as the embryos from the two groups cannot be distinguished. However, both sets were hybridized under the same conditions in parallel.

ES culture and differentiation

Mouse ES cells (E14TG2a, E14TG2a T-GFP) were maintained in GMEM media with 10% serum and leukaemia inhibitory factor (LIF) on gelatin-coated dishes. Differentiation assays were performed in DMEM/F12 and Neurobasal (1:1) medium with N2 and B27 (minus vitamin A, Invitrogen, 12587-010) supplements. Differentiation was initiated by embryoid body (EB) formation; 3×10^5 cells/ml were plated in individual wells of a six-well low-attachment (Corning/Sigma, CLS 3471) dish for 48 h. This was then followed by growth factor and small molecule treatments of EBs in suspension for differentiation assays. For muscle and heart differentiation, EB-derived spheres from the Xav+SB431542 or posterior culture conditions were plated on a dish with StemPro34SF media (for cardiac fate; Invitrogen, 10639011) and in DMEM with KnockOut Serum Replacement (ThermoFisher) supplemented with bovine serum albumin (for skeletal muscle). The concentrations of factors used are listed in Table S2.

Human ES cell differentiation: H9 cells (WiCell, SLA# 16-W0026) were cultured in mTESR1 (Stem Cell Technologies). Differentiation was induced using a protocol similar to mouse ESC differentiation that excludes the formation of embryoid bodies prior to small molecule/growth factor induction. Differentiation was carried out in chemically defined media (Vallier and Pedersen, 2008).

Ex utero mouse embryo culture

Wild-type embryos were collected at E7 and dissected in M2 media (Sigma). They were cultured on roller tubes in media (DMEM/F12 with Glutamax and penicillin-streptomycin) containing 50% rat serum (home-made) at 37°C, 5% O_2, 5% CO_2 for 22-24 h *ex utero* in the presence of DMSO (control) or CHIR99021 (8 µM).

Immunofluorescence and quantitation

For immunostaining, EB-derived 'mesoderm spheres' were stained in suspension. Quantitation of marker-positive nuclei was performed on optical sections through the spheres. For differentiation into cardiomyocytes and muscle, the spheres were plated. The attached cells originating from individual spheres aggregated into spheres and differentiated into big clusters of cardiomyocytes. Skeletal muscle differentiation also occurred in clusters and not uniformly in the dish. This precluded quantitation as the percentage marker-positive nuclei/cells in the population. We plated defined number of spheres per dish and each of these could be distinguished, as part of each sphere remained as a dome due to partial dispersal following attachment. Therefore, quantitative analysis measured the percentage of spheres associated with marker positive clusters of cells. For cultured cells, samples were fixed in 4% paraformaldehyde and washed with PBS. Permeabilization was carried out with 0.1% Triton-X in PBS followed by blocking in 5% normal donkey serum. Primary antibody was incubated overnight. This was followed by washes with 0.1% Tween-20 in PBS and incubation with secondary antibody. Cells were imaged following further washes with 0.1% Tween-20 in PBS. For whole-mount and EB-derived sphere immunostaining, samples were fixed in 4% paraformaldehyde and washed with 0.1% Tween-20 in PBS. Permeabilization was carried out using 0.3% Triton-X in PBS followed by blocking in 10% normal donkey serum. Primary antibody was incubated overnight. This was followed by washes with 0.1% Tween-20 in PBS and incubation with secondary antibody. Antibodies and dilutions are listed in Table S3. Olympus FluoView FV1000 confocal scanning microscope and software was used to acquire images. Optical sections (taken at 1-3 µm intervals) were *z*-stacked using ImageJ (NIH; Schneider et al., 2012). Statistical analysis for quantitation of marker-positive nuclei used one-way ANOVA followed by Tukey's post hoc test for multiple pairwise comparisons among differentiation conditions.

Quantitative RT-PCR

Total RNA (500 ng-1 µg) extracted using the Qiagen RNeasy Micropurification Kit was used to prepare cDNA (Super-Script III, Invitrogen). Oligo dT primers were used for cDNA synthesis from total RNA. Real-time PCR reactions were performed using PowerSYBR Green Universal Master Mix (Thermo Scientific) and analysed using ViiA7 Real Time PCR system (Applied Biosystems). Data were normalized using GAPDH expression. For all targets, primer efficiencies were calculated with serial dilutions of total cDNA and only those primer sets, which matched the efficiency of amplification of GAPDH internal reference primer set were used for the study. The specificity of the primers was also tested by melt curve. The primers are listed in Tables S4 and S5. Each condition was tested using two technical replicates and at least three biological replicates was analysed for relative gene expression using $2^{-\Delta\Delta Ct}$ method (Schmittgen and Livak, 2008). Error bars on all qPCR graphs represent s.e.m. Unpaired Student's *t*-tests (two-tailed) or one-way ANOVA followed by Dunnett's post hoc test for comparing individual inhibitor treatments to 'posterior' (many-to-one comparison) were performed.

Flow cytometric analysis

For flow analysis, the cells were stained with PE-conjugated anti-Flk1 and Superbright 436-conjugated anti-PDGFRα antibodies. Briefly, EBs derived

from E14Tg2a T-GFP cells (a gift from P. Chandra Shekar, CCMB, Hyderabad) were attached and differentiated by dual inhibition as described above. Following treatment, cells were dissociated with Accutase. The cell suspension was washed with 1× PBS+0.5% BSA. 1×10^6 cells in 100 µl suspension were stained with 0.5 µg Flk1 and 1 µg PDGFRα antibodies for 1 h, washed with 1×PBS+0.5% BSA three times. Live/death discrimination was carried out using 7-AAD (10 µg/ml). Analysis was performed using FACSVERSE (BD Scientific) and data analysed using FlowJo.

Western blotting

Protein (20 µg) samples were fractionated by electrophoresis on 10% SDS-PAGE gel, transferred on a nitrocellulose membrane (GE10600016, GE Healthcare), and incubated overnight at 4°C with primary antibodies and then with appropriate HRP-conjugated secondary antibodies (Table S3). ECL kit (32209, ThermoFisher Scientific) was used for visualization. Quantification of the bands was carried out using Fiji software. One-way ANOVA followed by Tukey's post hoc test was performed to analyse statistical significance.

Acknowledgements

We thank the animal facility (ACRC-NCBS/inStem), the Central Imaging and Flow Cytometry Facility, NCBS and the inStem Stem Cell Facility. We thank Upnishad Sharma and Payel Das for technical help, Dr Raj Ladher for critical reading of the manuscript and Profs Shahragim Tajbakhsh, Jyotsna Dhawan and Maneesha Inamdar, and Dr Michael Schubert for discussion.

Competing interests

The authors declare no competing or financial interests.

Author contributions

Conceptualization: R.S.; Methodology: N.N., B.V., A.J., R.S.; Validation: N.N., B.V.; Formal analysis: N.N., B.V., S.G., R.S.; Investigation: N.N., B.V., A.J., S.G.; Writing - original draft: R.S.; Writing - review & editing: N.N., B.V., A.J., R.S.; Visualization: N.N., B.V., A.J., S.G., R.S.; Supervision: R.S.; Project administration: R.S.; Funding acquisition: R.S.

Funding

N.N. is a Council of Scientific and Industrial Research (CSIR), India Senior Research Fellow (SRF); B.V. is a Department of Biotechnology, Ministry of Science and Technology, India SRF; A.J. receives a National Centre for Biological Sciences-Tata Institute of Fundamental Research PhD fellowship; S.G. is an InStem bridging postdoc fellow; and R.S. is a Ramalingaswami Fellow (BT/RLF/Re-entry/03/2010). The work is supported by Department of Biotechnology, Ministry of Science and Technology grants BT/PR13640/MED/97/263/2015 and BT/PR12017/MED/31/282/2014 to R.S. and by inStem. Animal work was partially supported by a Department of Biotechnology-NaMoR grant (BT/PR5981/MED/31/181/2012).

Supplementary information

Supplementary information available online at
http://dev.biologists.org/lookup/doi/10.1242/dev.160945.supplemental

References

Arkell, R. M. and Tam, P. P. L. (2012). Initiating head development in mouse embryos: integrating signalling and transcriptional activity. *Open Biol.* **2**, 120030.

Arnold, S. J. and Robertson, E. J. (2009). Making a commitment: cell lineage allocation and axis patterning in the early mouse embryo. *Nat. Rev. Mol. Cell Biol.* **10**, 91-103.

Aulehla, A. and Pourquie, O. (2010). Signaling gradients during paraxial mesoderm development. *Cold Spring Harb. Perspect. Biol.* **2**, a000869.

Behringer, R., Gertsenstein, M., Nagy, K. V. and Nagy, A. (2016). Differentiating mouse embryonic stem cells into embryoid bodies by hanging-drop cultures. *Cold Spring Harb. Protoc.* **2016**, 1073-1076.

Biben, C., Stanley, E., Fabri, L., Kotecha, S., Rhinn, M., Drinkwater, C., Lah, M., Wang, C.-C., Nash, A., Hilton, D. et al. (1998). Murine cerberus homologue mCer-1: a candidate anterior patterning molecule. *Dev. Biol.* **194**, 135-151.

Bothe, I. and Dietrich, S. (2006). The molecular setup of the avian head mesoderm and its implication for craniofacial myogenesis. *Dev. Dyn.* **235**, 2845-2860.

Buckingham, M. (2017). Gene regulatory networks and cell lineages that underlie the formation of skeletal muscle. *Proc. Natl. Acad. Sci. USA* **114**, 5830-5837.

Burridge, P. W., Keller, G. M., Gold, J. D. and Wu, J. C. (2013). Production of de novo cardiomyocytes: human pluripotent stem cell differentiation and direct reprogramming. *Cell Stem Cell* **10**, 16-28.

Cao, N., Liu, Z., Chen, Z., Wang, J., Chen, T., Zhao, X., Ma, Y., Qin, L., Kang, J., Wei, B. et al. (2012). Ascorbic acid enhances the cardiac differentiation of induced pluripotent stem cells through promoting the proliferation of cardiac progenitor cells. *Cell Res.* **22**, 219-236.

Chal, J., Oginuma, M., Al Tanoury, Z., Gobert, B., Sumara, O., Hick, A., Bousson, F., Zidouni, Y., Mursch, C., Moncuquet, P. et al. (2015). Differentiation of pluripotent stem cells to muscle fiber to model Duchenne muscular dystrophy. *Nat. Biotechnol.* **33**, 962-969.

Chan, S. S.-K., Hagen, H. R., Swanson, S. A., Stewart, R., Boll, K. A., Aho, J., Thomson, J. A. and Kyba, M. (2016). Development of bipotent cardiac/skeletal myogenic progenitors from MESP1+ mesoderm. *Stem Cell Rep.* **6**, 26-34.

Chapman, D. L. and Papaioannou, V. E. (1998). Three neural tubes in mouse embryos with mutations in the T-box gene Tbx6. *Nature* **391**, 695-697.

Chapman, D. L., Agulnik, I., Hancock, S., Silver, L. M. and Papaioannou, V. E. (1996). Tbx6, a mouse T-Box gene implicated in paraxial mesoderm formation at gastrulation. *Dev. Biol.* **180**, 534-542.

Ciruna, B. G., Schwartz, L., Harpal, K., Yamaguchi, T. P. and Rossant, J. (1997). Chimeric analysis of fibroblast growth factor receptor-1 (Fgfr1) function: a role for FGFR1 in morphogenetic movement through the primitive streak. *Development* **124**, 2829-2841.

Couly, G. F., Coltey, P. M. and Le Douarin, N. M. (1992). The developmental fate of the cephalic mesoderm in quail-chick chimeras. *Development* **114**, 1-15.

Deng, C., Bedford, M., Li, C., Xu, X., Yang, X., Dunmore, J., and Leder, P. (1997). Fibroblast growth factor receptor-1 (FGFR-1) is essential for normal neural tube and limb development. *Dev. Biol* **185**, 42-54.

Diogo, R., Kelly, R. G., Christiaen, L., Levine, M., Ziermann, J. M., Molnar, J. L., Noden, D. M. and Tzahor, E. (2015). A new heart for a new head in vertebrate cardiopharyngeal evolution. *Nature* **520**, 466-473.

DiRenzo, D. M., Chaudhary, M. A., Shi, X., Franco, S. R., Zent, J., Wang, K., Guo, L.-W. and Kent, K. C. (2016). A crosstalk between TGF-β/Smad3 and Wnt/β-catenin pathways promotes vascular smooth muscle cell proliferation. *Cell Signal.* **28**, 498-505.

Evans, D. J. R. and Noden, D. M. (2006). Spatial relations between avian craniofacial neural crest and paraxial mesoderm cells. *Dev. Dyn.* **235**, 1310-1325.

Galceran, J., Fariñas, I., Depew, M. J., Farin, I., Clevers, H. and Grosschedl, R. (1999). Wnt3a−/− like phenotype and limb deficiency in Lef1−/− Tcf1−/− mice. *Genes Dev.* **15**, 709-717.

Gans, C. and Northcutt, R. G. (1983). Neural crest and the origin of vertebrates: a new head. *Science* **220**, 268-273.

Gonsalves, F. C., Klein, K., Carson, B. B., Katz, S., Ekas, L. A., Evans, S., Nagourney, R., Cardozo, T., Brown, A. M. and DasGupta, R. (2011). An RNAi-based chemical genetic screen identifies three small-molecule inhibitors of the Wnt/wingless signaling pathway. *Proc. Natl. Acad. Sci. USA* **108**, 5954-5963.

Grifone, R. and Kelly, R. G. (2007). Heartening news for head muscle development. *Trends Genet.* **23**, 365-369.

Guo, X. and Wang, X.-F. (2009). Signaling cross-talk between TGF-β/BMP and other pathways. *Cell Res.* **19**, 71-88.

Hacker, A. and Guthrie, S. (1998). A distinct developmental programme for the cranial paraxial mesoderm in the chick embryo. *Development* **125**, 3461-3472.

Harel, I., Nathan, E., Tirosh-Finkel, L., Zigdon, H., Guimarães-Camboa, N., Evans, S. M. and Tzahor, E. (2009). Distinct origins and genetic programs of head muscle satellite cells. *Dev. Cell* **16**, 822-832.

Henrique, D., Adam, J., Myat, A., Chitnis, A., Lewis, J. and Ish-Horowicz, D. (1995). Expression of a Delta homologue in prospective neurons in the chick [see comments]. *Nature* **375**, 787-790.

Herrmann, B. G. (1991). Expression pattern of the Brachyury gene in whole-mount TWis/TWis mutant embryos. *Proc. Natl. Acad. Sci. USA* **113**, 913-917.

Ip, C. K., Fossat, N., Jones, V., Lamonerie, T, and Tam, P. P. (2014). Head formation: OTX2 regulates Dkk1 and Lhx1 activity in the anterior mesendoderm. *Development* **141**, 3859-3867.

Javali, A., Misra, A., Leonavicius, K., Acharyya, D., Vyas, B. and Sambasivan, R. (2017). Co-expression of Tbx6 and Sox2 identifies a novel transient neuromesoderm progenitor cell state. *Development* **144**, 4522-4529.

Jho, E., Zhang, T., Domon, C., Joo, C.-K., Freund, J.-N. and Costantini, F. (2002). Wnt/β-Catenin/Tcf signaling induces the transcription of Axin2, a negative regulator of the signaling pathway. *Mol. Cell. Biol.* **22**, 1172-1183.

Jiwlawat, N., Lynch, E., Jeffrey, J., Van Dyke, J. M. and Suzuki, M. (2018). Current progress and challenges for skeletal muscle differentiation from human pluripotent stem cells using transgene-free approaches. *Stem Cells Int.* **2018**, 1-18.

Kataoka, H., Takakura, N., Nishikawa, S., Tsuchida, K., Kodama, H., Kunisada, T., Risau, W., Kita, T. and Nishikawa, S.-I. (1997). Expressions of PDGF receptor alpha, c-Kit and Flk1 genes clustering in mouse chromosome 5 define distinct subsets of nascent mesodermal cells. *Dev. Growth Differ.* **39**, 729-740.

Kattman, S. J., Witty, A. D., Gagliardi, M., Dubois, N. C., Niapour, M., Hotta, A., Ellis, J. and Keller, G. (2011). Stage-specific optimization of activin/nodal and BMP signaling promotes cardiac differentiation of mouse and human pluripotent stem cell lines. *Cell Stem Cell* **8**, 228-240.

Keller, G. (2005). Embryonic stem cell differentiation: emergence of a new era in biology and medicine. *Genes Dev.* **19**, 1129-1155.
Kelly, R. G., Brown, N. A. and Buckingham, M. E. (2001). The arterial pole of the mouse heart forms from Fgf10-expressing cells in pharyngeal mesoderm. *Dev. Cell* **1**, 435-440.
Kelly, R. G., Jerome-Majewska, L. A. and Papaioannou, V. E. (2004). The del22q11.2 candidate gene Tbx1 regulates branchiomeric myogenesis. *Hum. Mol. Genet.* **13**, 2829-2840.
Kokkinopoulos, I., Ishida, H., Saba, R., Coppen, S., Suzuki, K. and Yashiro, K. (2016). Cardiomyocyte differentiation from mouse embryonic stem cells using a simple and defined protocol. *Dev. Dyn.* **245**, 157-165.
Lawson, K. A., Meneses, J. J. and Pedersen, R. A. (1991). Clonal analysis of epiblast fate during germ layer formation in the mouse embryo. *Development* **113**, 891-911.
Lescroart, F., Kelly, R. G., Le Garrec, J.-F., Nicolas, J.-F., Meilhac, S. M. and Buckingham, M. (2010). Clonal analysis reveals common lineage relationships between head muscles and second heart field derivatives in the mouse embryo. *Development* **137**, 3269-3279.
Lescroart, F., Chabab, S., Lin, X., Rulands, S., Paulissen, C., Rodolosse, A., Auer, H., Achouri, Y., Dubois, C., Bondue, A. et al. (2014). Early lineage restriction in temporally distinct populations of Mesp1 progenitors during mammalian heart development. *Nat. Cell Biol.* **16**, 829-840.
Lescroart, F., Hamou, W., Francou, A., Théveniau-Ruissy, M., Kelly, R. G. and Buckingham, M. (2015). Clonal analysis reveals a common origin between nonsomite-derived neck muscles and heart myocardium. *Proc. Natl. Acad. Sci. USA* **112**, 1446-1451.
Lewis, S. L., Khoo, P.-L., De Young, R. A., Steiner, K., Wilcock, C., Mukhopadhyay, M., Westphal, H., Jamieson, R. V., Robb, L. and Tam, P. P. L. (2008). Dkk1 and Wnt3 interact to control head morphogenesis in the mouse. *Development* **135**, 1791-1801.
Lu, J.-R., Bassel-Duby, R., Hawkins, A., Chang, P., Valdez, R., Wu, H., Gan, L., Shelton, J. M., Richardson, J. A. and Olson, E. N. (2002). Control of facial muscle development by MyoR and capsulin. *Science* **298**, 2378-2381.
Martin, L. B. and Kimelman, D. (2012). Canonical Wnt signaling dynamically controls multiple stem cell fate decisions during vertebrate body formation. *Development* **22**, 223-232.
Marvin, M. J., Rocco, G., Di Gardiner, A., Bush, S. M. and Lassar, A. B. (2001). Inhibition of Wnt activity induces heart formation from posterior mesoderm. *Genes Dev.* **15**, 316-327.
Mendjan, S., Mascetti, V. L., Ortmann, D., Ortiz, M., Karjosukarso, D. W., Ng, Y., Moreau, T. and Pedersen, R. A. (2014). NANOG and CDX2 pattern distinct subtypes of human mesoderm during exit from pluripotency. *Cell Stem Cell* **15**, 310-325.
Morkel, M., Huelsken, J., Wakamiya, M., Ding, J., van de Wetering, M., Clevers, H., Taketo, M. M., Behringer, R. R., Shen, M. M. and Birchmeier, W. (2003). β-Catenin regulates Cripto- and Wnt3-dependent gene expression programs in mouse axis and mesoderm formation. *Development* **130**, 6283-6294.
Naiche, L. A., Holder, N. and Lewandoski, M. (2011). FGF4 and FGF8 comprise the wavefront activity that controls somitogenesis. *Proc. Natl. Acad. Sci. USA* **108**, 4018-4023.
Nathan, E., Monovich, A., Tirosh-Finkel, L., Harrelson, Z., Rousso, T., Rinon, A., Harel, I., Evans, S. M. and Tzahor, E. (2008). The contribution of Islet1-expressing splanchnic mesoderm cells to distinct branchiomeric muscles reveals significant heterogeneity in head muscle development. *Development* **135**, 647-657.
Niehrs, C. (2010). On growth and form: a Cartesian coordinate system of Wnt and BMP signaling specifies bilaterian body axes. *Development* **137**, 845-857.
Onai, T., Aramaki, T., Inomata, H., Hirai, T. and Kuratani, S. (2015). Ancestral mesodermal reorganization and evolution of the vertebrate head. *Zool. Lett.* **1**, 29.
Perea-gomez, A., Vella, F. D. J., Shawlot, W., Oulad-abdelghani, M., Chazaud, C., Meno, C., Pfister, V., Chen, L., Robertson, E., Hamada, H. et al. (2002). Nodal antagonists in the anterior visceral endoderm prevent the formation of multiple primitive streaks. *Dev. Cell* **3**, 745-756.
Petersen, C. P. and Reddien, P. W. (2009). Wnt signaling and the polarity of the primary body axis. *Cell* **139**, 1056-1068.
Piccolo, S., Aguis, E., Leyns, L., Bhattacharyya, S., Grunz, H., Bouwmeester, T. and De Robertis, E. M. (1999). The head inducer Cerberus is a multifunctional antagonist of Nodal, BMP and Wnt signals. *Nature* **397**, 707-710.
Ramkumar, N. and Anderson, K. V. (2011). SnapShot: mouse primitive streak. *Cell* **146**, 488-488.e2.
Rodríguez-Esteban, C., Capdevila, J., Kawakami, Y. and Belmonte, J. C. I. (2001). Wnt signaling and PKA control Nodal expression and left-right determination in the chick embryo. *Development* **128**, 3189-3195.
Sambasivan, R., Gayraud-Morel, B., Dumas, G., Cimper, C., Paisant, S., Kelly, R. G. and Tajbakhsh, S. (2009). Distinct regulatory cascades govern extraocular and pharyngeal arch muscle progenitor cell fates. *Dev. Cell* **16**, 810-821.
Sambasivan, R., Kuratani, S. and Tajbakhsh, S. (2011). An eye on the head: the development and evolution of craniofacial muscles. *Development* **138**, 2401-2415.
Schmittgen, T. D. and Livak, K. J. (2008). Analyzing real-time PCR data by the comparative C(T) method. *Nat. Protoc.* **3**, 1101-1108.
Schneider, V. A. and Mercola, M. (2001). Wnt antagonism initiates cardiogenesis in Xenopus laevis. *Genes Dev.* **15**, 304-315.
Schneider, C. A., Rasband, W. S. and Eliceiri, K. W. (2012). NIH Image to ImageJ: 25 years of image analysis. *Nat. Methods* **9**, 671-675.
Shih, H. P., Gross, M. K. and Kioussi, C. (2008). Muscle development: forming the head and trunk muscles. *Acta Histochem.* **110**, 97-108.
Skromne, I. and Stern, C. D. (2001). Interactions between Wnt and Vg1 signalling pathways initiate primitive streak formation in the chick embryo. *Development* **128**, 2915-2927.
Stolfi, A., Gainous, T. B., Young, J. J., Mori, A., Levine, M. and Christiaen, L. (2010). Early chordate origins of the vertebrate second heart field. *Science* **329**, 565-568.
Stower, M. J. and Srinivas, S. (2014). Heading forwards: anterior visceral endoderm migration in patterning the mouse embryo. *Philos. Trans. R. Soc. B Biol. Sci.* **369**, 20130546-20130546.
Swartz, E. W., Baek, J., Pribadi, M., Wojta, K. J., Almeida, S., Karydas, A., Gao, F.-B., Miller, B. L. and Coppola, G. (2016). A novel protocol for directed differentiation of C9orf72-associated human induced pluripotent stem cells into contractile skeletal myotubes. *Stem Cells Transl. Med.* **5**, 1461-1472.
Tajbakhsh, S., Rocancourt, D., Cossu, G. and Buckingham, M. (1997). Redefining the genetic hierarchies controlling skeletal myogenesis: Pax-3 and Myf-5 act upstream of MyoD. *Cell* **89**, 127-138.
Takahashi, T., Lord, B., Schulze, P. C., Fryer, R. M., Sarang, S. S., Gullans, S. R. and Lee, R. T. (2003). Ascorbic acid enhances differentiation of embryonic stemcells into cardiac myocytes. *Circulation* **107**, 1912-1917.
Tam, P. P. and Beddington, R. S. (1987). The formation of mesodermal tissues in the mouse embryo during gastrulation and early organogenesis. *Development* **99**, 109-126.
Thomas, P. and Beddington, R. (1996). Anterior primitive endoderm may be responsible for patterning the anterior neural plate in the mouse embryo. *Curr. Biol.* **6**, 1487-1496.
Tirosh-Finkel, L., Elhanany, H., Rinon, A. and Tzahor, E. (2006). Mesoderm progenitor cells of common origin contribute to the head musculature and the cardiac outflow tract. *Development* **133**, 1943-1953.
Turner, D. A., Hayward, P. C., Baillie-johnson, P., Rué, P., Broome, R. and Faunes, F. (2014). Wnt/β-catenin and FGF signalling direct the specification and maintenance of a neuromesodermal axial progenitor in ensembles of mouse embryonic stem cells. *Development* **141**, 4243-4253.
Tzahor, E. and Evans, S. M. (2011). Pharyngeal mesoderm development during embryogenesis: Implications for both heart and head myogenesis. *Cardiovasc. Res.* **91**, 196-202.
Tzahor, E., Kempf, H., Mootoosamy, R. C., Poon, A. C., Abzhanov, A., Tabin, C. J., Dietrich, S. and Lassar, A. B. (2003). Antagonists of Wnt and BMP signaling promote the formation of vertebrate head muscle. *Genes Dev.* **17**, 3087-3099.
Vallier, L. and Pedersen, R. A. (2008). Differentiation of human embryonic stem cells in adherent and in chemically defined culture conditions. *Curr. Protoc. Stem Cell Biol.* **4**, 1D.4.1-1D.4.7.
Wachtler, F. and Jacob, M. (1986). Origin and development of the cranial skeletal muscles. *Bibl thca Anat.* **29**, 24-46.
Yamaguchi, T. P., Takada, S., Yoshikawa, Y., Wu, N. and McMahon, A. P. (1999). T (Brachyury) is a direct target of Wnt3a during paraxial mesoderm specification. *Genes Dev.* **13**, 3185-3190.
Yamamoto, M., Saijoh, Y., Perea-gomez, A., Shawlot, W., Behringer, R. R. and Ang, S. (2004). Nodal antagonists regulate formation of the anteroposterior axis of the mouse embryo. *Nature* **428**, 387-392.
Yang, L., Soonpaa, M. H., Adler, E. D., Roepke, T. K., Kattman, S. J., Kennedy, M., Henckaerts, E., Bonham, K., Abbott, G. W., Linden, R. M. et al. (2008). Human cardiovascular progenitor cells develop from a KDR+ embryonic-stem-cell-derived population. *Nature* **453**, 524-528.

Supplementary Tables:

Table S1. Source of mouse strains used in the study

Strain	Reference	Our source
Tg:Axin2-d2EGFP	Jho et al., 2002	Tole, S., DBS, TIFR-Mumbai
Mesp1^{Cre}	Saga et al., 1999	Meilhac, S., Institut Imagine, Paris
Tg:Tbx6-Cre	Javali et al., 2017	Generated by us
Tbx6$^{H2B\text{-}EYFP}$	Hadjantonakis et al., 2008	Papaioannou, V., Columbia University Medical Center, New York Stock# 004591
T^{Wis}	Shedlovsky et al., 1988	The Jackson Laboratory, USA Stock# 007676
ROSA^{mTmG}	Muzumdar et al., 2007	The Jackson Laboratory, USA
ROSA^{nlacZ}	Tzouanacou et al., 2009	Tajbakhsh, S., Institut Pasteur, Paris
Myf5^{nlacZ}	Tajbakhsh et al., 1997	Tajbakhsh, S., Institut Pasteur, Paris
Pax7^{GPL}	Sambasivan et al., 2009	Tajbakhsh, S., Institut Pasteur, Paris

Table S2. Small molecules and growth factors

Name	Company	Catalog no.	Concentration
Activin A	R&D	338-AC-050	20 ng/mL
Ascorbic Acid	SIGMA	4403-100MG	0.5 mM
Bmp4	R&D	314-BP-010	10 ng/mL
CHIR99021	Tocris	4423/10	8 μM
Dkk1	R&D	5439-DK-010	150 ng/mL
FGF2	Peprotech	AF-100-18B-100	5-20 ng/mL
Fgf10	R&D	345-FG-025	50 ng/mL
HGF	R&D	2207-HG-025	10 ng/mL
iCRT3	SIGMA	SML0211-5MG	10 μM
iCRT5	Abcam	ab142141	50 μM
IGF-1	Peprotech	250-19-10	2 ng/mL
LDN193189	Stemcell	72142	0.1 μM
SB431542	Tocris	1614/10	10 μM
VEGF	R&D	493-MV-005	5 ng/mL
Xav939	SIGMA	X3004-5MG	5 μM

Table S3. Antibody sources and dilutions

Antigen	Company	Catalog no.	Dilution (IF)	Dilution (WB)	Dilution (FACS)
7-Aminoactinomycin D	ThermoFisher Scientific	A1310			10μg/mL
α-Actinin	SIGMA	A7811	1:200		
β-actin	SIGMA	A5316-.2ML		1:500	
β-catenin	Abcam	ab16051		1:2500	
CD31	BD	550274	1:200		
cardiact TroponinI	Abcam	ab47003	1:120		
cardiac TroponinT	ThermoFisher Scientific	MA5-12960	1:200		
Desmin	SIGMA	D1033	1:40		
Eomes	Abcam	ab23345	1:200		
Flk-1/CD309	ThermoFisher Scientific	12-5821-82			0.5μg / 10^6 cells
GFP	Abcam	ab13970	1:300		
Isl1	DSHB	40.2D6	1:100		
Myod	Dako	M351201-2	1:100		
Myogenin	DSHB	F5D	1:10		
Myosin heavy chain (Skeletal muscle specific)	SIGMA	M4276	1:100		
Nkx2.5	ThermoFisher Scientific	PA5-49431	1:50		
Oct3/4	SantaCruz Biotechnology	sc-8628	3μg/mL		
PDGFRα/CD140a	ThermoFisher Scientific	62-1401-82			1.0μg / 10^6 cells
phospho-Smad2	Cell Signaling Technologies	3108S		1:1000	
Pax3	DSHB	C1-575	1:150		
Sox2	SantaCruz Biotechnology	sc17320	1:67		
Total Smad2/3	Cell Signaling Technologies	5678S		1:1000	
T/Brachyury	SantaCruz Biotechnology	sc-17743	3μg/mL		
Tbx1	Abcam	ab18530	1:100		
Tbx1	ThermoFisher Scientific	PA5-26389	1:100		
Tbx6	Imagenex	custom generated			

Table S4. Mouse RT-qPCR primers

Gene	Primer	Reference
Axin2	AGGAGCAGCTCAGCAAAAAG GCTCAGTCGATCCTCTCCAC	Kurek *et al*, Stem Cell Reports, 2015
Cdx1	GCGTTGGTGGTCTGTGTAGA ACGCCCTACGAATGGATG	qPCR Primer Depot
Cdx2	TCAACCTCGCCACAACCTTCCC TGGCTCAGCCTGGGATTGCT	Rayon *et al*, Dev Cell, 2014
Cdx4	AAATTCCTTTTCCAGCTCCA ATGGATGCGCAAAACTGTG	qPCR Primer Depot
cTnT	CAAGGAGCTGTGGCAGAGTA TTCTGGTTGTCATTGATCCG	Kokkinopoulos *et al*, Dev Dyn, 2015
CYP26a1	AGCTGTTCCAAAGTTTCCATGT ACCCACATGTCCTCCAGAAA	qPCR Primer Depot
Fgf10	GTTGCTGTTGATGGCTTTGA GATTGAGAAGAACGGCAAGG	qPCR Primer Depot
Foxa2	TCATGTTGCTCACGGAAGAG TAAAGTATGCTGGGAGCCGT	qPCR Primer Depot
Hand1	CTTTAATCCTCTTCTCGCCG TGAACTCAAAAAGACGGATGG	qPCR Primer Depot
Isl1	CACGAAGTCGTTCTTGCTGA GGTTAGGGATGGGAAAACCT	Caprio *et al*, PNAS, 2014
Kdr	TCCAGAATCCTCTTCCATGC AAACCTCCTGCAAGCAAATG	qPCR Primer Depot
Lhx2	CCAGCTTCGGACAATGAAGT TTTCCTGCCGTAAAAGGTTG	Harel *et al*, PNAS, 2012
Mixl1	ACTTTCCAGCTCTTTCAAGAGCC ATTGTGTACTCCCCAACTTTCCC	Costello *et al*, Nature Letters, 2011
Mlc2v	AGGGTCACTGAAGGCTGACT GGTCGATCTCCTCTTTGGAG	Kokkinopoulos *et al*, Dev Dyn, 2015
Msc	ACATTCACCCAGTCAACCTG CCACTTCCTTCAGGTCATTCTC	Sambasivan *et al*, Dev Cell, 2009
Msgn1	CTCTGCTTTTCCAGTCCCAG AACCTGGGTGAGACCTTCCT	qPCR Primer Depot
Myf5	GACAGGGCTGTTACATTCAGG TGAGGGAACAGGTGGAGAAC	qPCR Primer Depot
MyoD	GTCGTAGCCATTCTGCCG AGCACTACAGTGGCGACTCA	qPCR Primer Depot
MyoG	GTGGGAGTTGCATTCACTGG CTACAGGCCTTGCTCAGCTC	qPCR Primer Depot
Nanog	AAAGGATGAAGTGCAAGCG TCTGGCTGCTCCAAGTT	Kurek *et al*, Stem Cell Reports, 2015
Nkx2.5	AAGCAACAGCGGTACCTGTC GCTGTCGCTTGCACTTGTAG	Shelton *et al*, Stem Cell Reports, 2014

Oct4	GAACATGTGTAAGCTGCGG CAGACTCCACCTCACACG	Kurek *et al*, Stem Cell Reports, 2015
Otx2	GAAAATCAACTTGCCAGAATCCA GCGGCACTTAGCTCTTCGAT	Iwafuchi-Doi, Development, 2012
Pitx2	TGTCCACTCGCGAAGAAATC AAGCCATTCTTGCACAGCTC	Sambasivan *et al*, Dev Cell, 2009
RALDH2	GCTCTCCTGTGGCTGGATTA GCCCAACCTCGAGATCAAGT	qPCR Primer Depot
Sox17	TCTTGGGGAAATAGGAAGGC TGGAACCTCCAGTAAGCCAG	qPCR Primer Depot
Sox2	AGCTCGCAGACCTACATGAA CCCTGGAGTGGGAGGAA	Kurek *et al*, Stem Cell Reports, 2015
T/Bra	CATGTACTCTTTCTTGCTGG GGTCTCGGGAAAGCAGTGGC	Lolas *et al*, PNAS, 2014
Tbx1	TGTGGGACGAGTTCAATCAG TGTCATCTACGGGCACAAAG	Sambasivan *et al*, Dev Cell, 2009
Tbx1 (Set 2)	CATGAGCAGCATGTAGTCGG TGTGGGACGAGTTCAATCAG	qPCR Primer Depot
Tbx5	TGGTTGGAGGTGACTTTGTG GGCAGTGATGACCTGGAGTT	qPCR Primer Depot
Tbx6	GTGTATCCCCACTCCCACAG CCGAGAAAATGGCAGAAACT	qPCR Primer Depot
Tcf21	CTGTAGTTCCACACAAGCGG CGGTTACATTCACCCAGTCA	qPCR Primer Depot

Table S5. Human RT-qPCR primers

Gene	Primer	Reference
Axin2	CTGGTGCAAAGACATAGCCA AGTGTGAGGTCCACGGAAAC	qPCR Primer Depot
Isl1	CGCATTTGATCCCGTACAAC GGTTTCTCCGGATTTGGAAT	Harel *et al*, PNAS, 2012
Mixl1	CCGAGTCCAGGATCCAGGTA CTCTGACGCCGAGACTTGG	Mendjan *et al*, Cell Stem Cell, 2014
Msgn1	AGAGGGAGAAGCTCAGGATGAG GTGTCTGGATCTTGGTGAGAGG	qPCR Primer Depot
Nanog	TTGGGACTGGTGGAAGAATC GATTTGTGGGCCTGAAGAAA	qPCR Primer Depot
Nkx2.5	AGCTCATAGACCTGCGCCT AGGACCCTAGAGCCGAAAAG	qPCR Primer Depot
Oct4	CTGGTTCGCTTTCTCTTTCG CTTTGAGGCTCTGCAGCTTA	qPCR Primer Depot
Otx2	GCTGTTGTTGCTGTTGTTGG AGAGGAGGTGGCACTGAAAA	qPCR Primer Depot
Sox2	GGAAAGTTGGGATCGAACAA GCGAACCATCTCTGTGGTCT	qPCR Primer Depot
T/Bra	TATGAGCCTCGAATCCACATAGT CCTCGTTCTGATAAGCAGTCAC	qPCR Primer Depot
Tbx1	CAGCTTTCACTTCCTTGTCCT ACCCTGAGGACTGGCCC	Harel *et al*, PNAS, 2012
Tbx6	AGCCTGTGTCTTTCCATCGT GCTGCCCGAACTAGGTGTAT	Mendjan *et al*, Cell Stem Cell, 2014
Tcf21	TTCAGGTCACTCTCGGGTTT AGCTACATCGCCCACTTGAG	Harel *et al*, PNAS, 2012
Twist1	TCCATTTTCTCCTTCTCTGGAA GGCTCAGCTACGCCTTCTC	qPCR Primer Depot

Supplementary Figures:

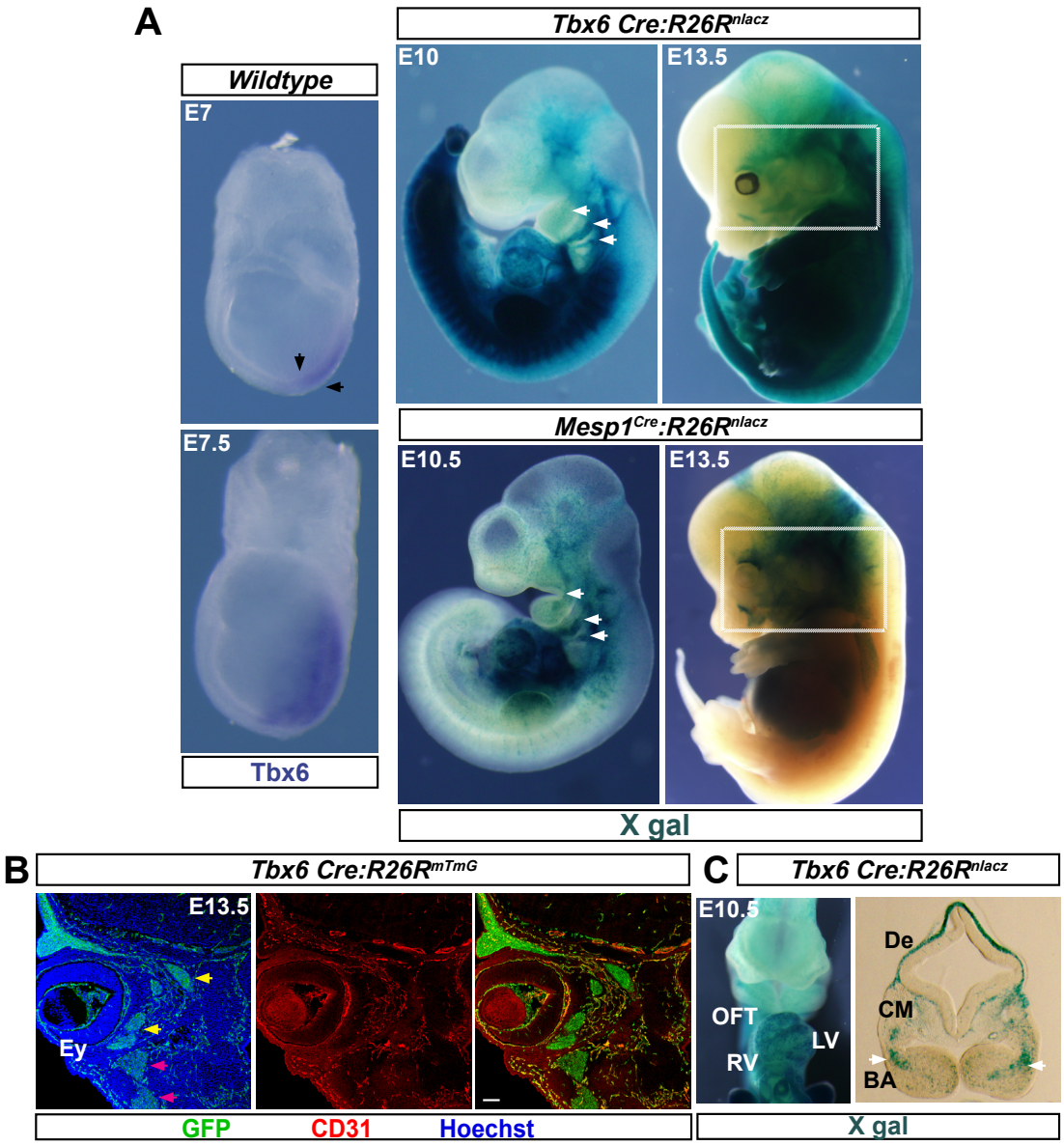

Figure S1: *Tbx6*-lineage trace marks head mesoderm including its head muscle derivatives. A) Wholemount ISH (left) on gastrulating mouse embryos. Black arrows, anterior primitive streak. Note, expression in the anterior primitive streak, the source of head mesoderm progenitors. Right panel shows X-gal stained littermates. White arrows, pharyngeal arch-derived muscles; White box highlights head mesoderm derivatives. *Mesp1*^{Cre} serves as an example of head mesoderm lineage reporter. B) Immunostaining of a coronal sections of E13.5 head. Note, *Tbx6-Cre* mediated GFP expression in extraocular (yellow arrows) as well as 1st and 2nd arch muscle progenitors (pink arrows). CD31 co-staining reveals endothelia marked by *Tbx6*-lineage. Scale bar 50 µm. C) *Tbx6-Cre* also marks the anterior-most mesoderm, heart, including the first (left ventricle, LV) and second heart field derivatives (Outflow tract, OFT; right ventricle, RV). Repeats are at least 3 embryos and 2 litters.

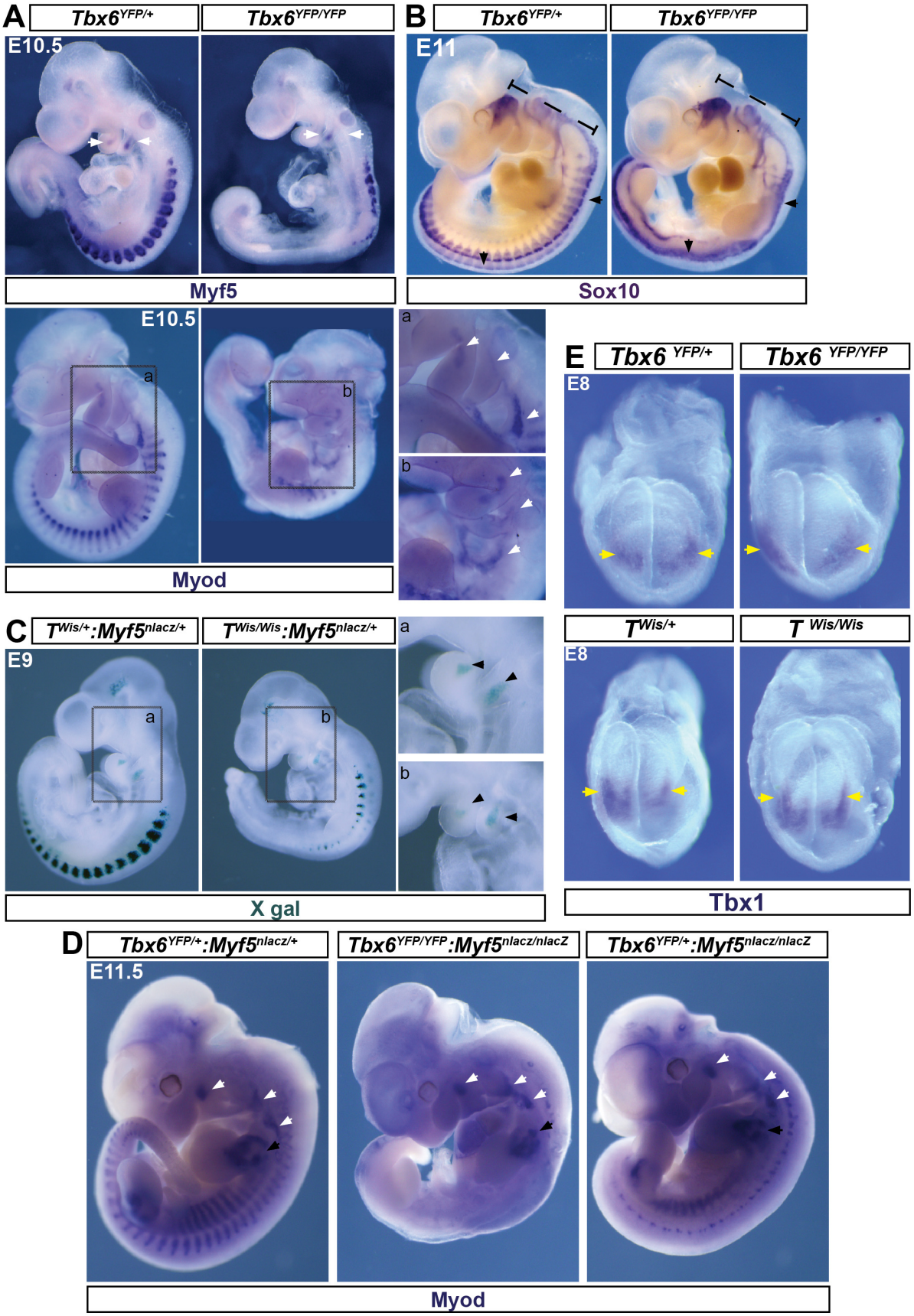

Figure S2: *T* and *Tbx6* dispensable for head mesoderm and head muscle development unlike that of posterior somitic mesoderm. A) ISH of littermate embryos. Since neural crest patterning is mesoderm-dependent, neural crest gene *Sox10* serves as an indirect marker of mesoderm development. *Sox10* reveals severe failure to pattern dorsal root ganglia from trunk neural crest (black arrows), while head mesoderm-dependent cranial ganglia appears to pattern and develop normally (dashed line). Note, although the cervical somites are formed in the mutants, the dorsal root ganglia from the neural crest are not patterned. For all ISH, n = 3 mutant embryos, at least. B) ISH of littermate embryos. *Myf5* RNA expression correlates with *Myf5* reporter expression data shown in Figure 1. ISH for *Myod* shows unperturbed progression in myogenic lineage in the pharyngeal arches (white arrowheads). C) Wholemount X gal staining of littermate embryos. No apparent delay in induction of *Myf5* reporter in the pharyngeal arches (black arrowheads). Note, *T* as well as *Tbx6* null mutants shown in A and C are slightly developmentally delayed compared to heterozygous littermates. Accounting for this age difference, the induction of *Myf5* reporter and *Myod* in arch muscle progenitors in mutants appear comparable to that in heterozygote or wildtype controls. D) ISH for *Myod* shows unperturbed progression in myogenic lineage in the pharyngeal arches (white arrowheads) in double nulls compared to age-matched controls. Note, the muscle anlage in the forelimb (black arrowheads) are also formed as in control embryos suggesting unaffected development of migratory muscle progenitors from cervical somites. E) ISH shows unperturbed *Tbx1* induction in a subset of early head mesoderm (yellow arrowheads).

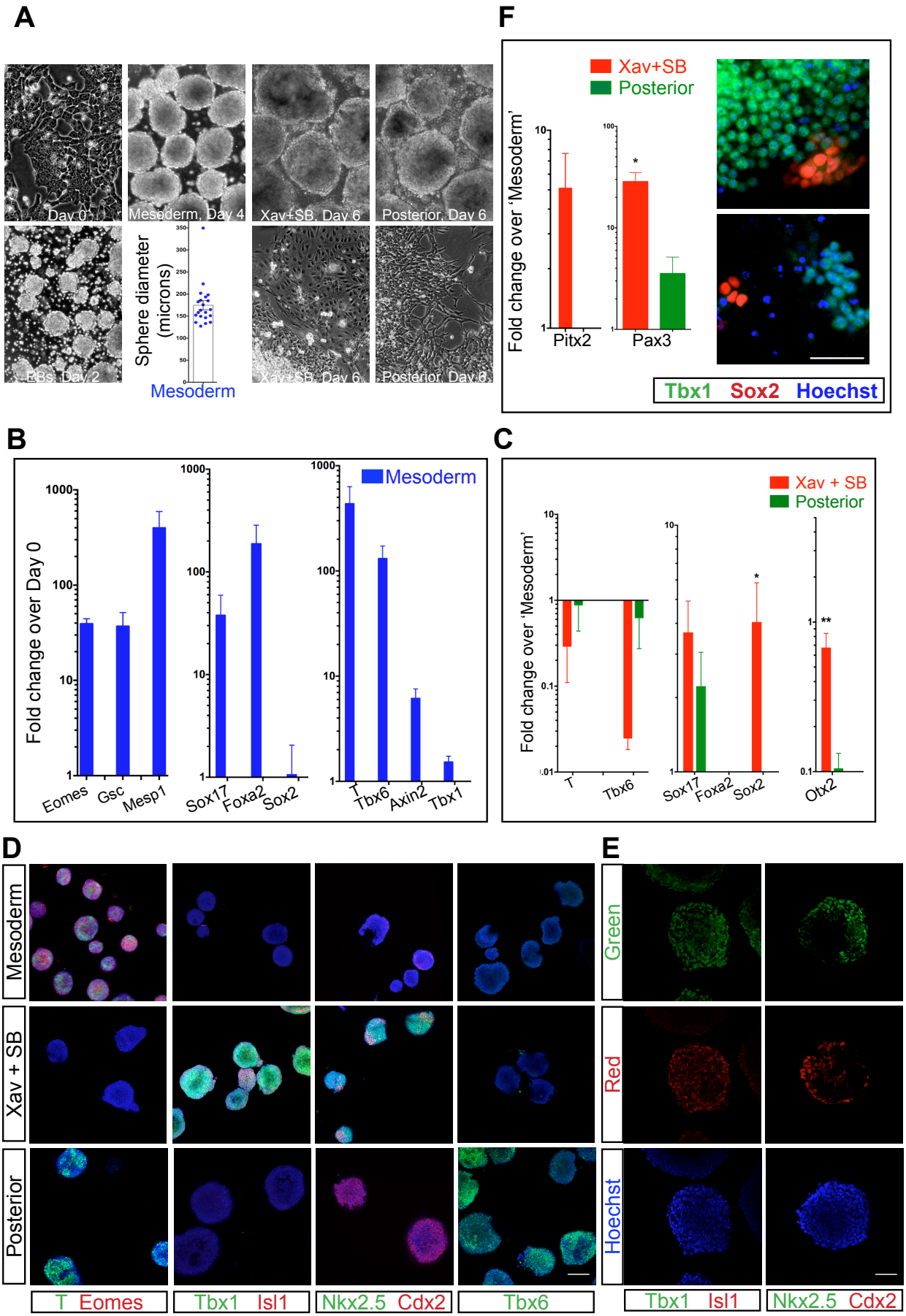

Figure S3: Inhibition of Wnt and Nodal in cardiopharyngeal mesoderm marker induction.
A) Micrographs of cultures during the course of differentiation. The panels show embryoid bodies (EBs) and differentiated spheres derived from EBs. The last two panels in the bottom row show corresponding adherent cultures plated on Day 4.
Diameter of Mesoderm spheres in microns: 174.7 ± 10.4 (mean ± SEM). n=21 spheres.
B) RT-qPCR analysis for early anterior streak markers (Eomes, Gsc, Mesp1), endoderm (Sox17, Foxa2), neurectoderm (Sox2) and mesoderm (T, Tbx6) markers in 'Mesoderm' condition over Day0. Induction of Wnt pathway is inferred by Axin2 expression.
C) RT-qPCR analysis for mesoderm (T, Tbx6), endoderm (Sox17, Foxa2), neurectoderm (Sox2) and anterior (Otx2) markers at Xav+SB or Posterior, when compared to 'Mesoderm'.
D) View of a larger field of the immunostaining assay. Oct4, pluripotency marker. T, Eomes, mesoderm markers. Tbx1, Isl1, Nkx2.5 cardiopharyngeal mesoderm markers. Tbx6, Cdx2, posterior mesoderm markers. Scale bars 200 μm.
E) Split channel view of CPM markers (Tbx1, Isl1, Nkx2.5) and Posterior marker Cdx2 at Xav+SB. For merged image see Fig. 4B. Scale bar 50 μm.
F) RT-qPCR data shows induction of Pitx2 and Pax3 in Xav+SB. In the mouse embryos, initially *Pitx2* marks premandibular mesoderm, but is induced later in somites as well (L'Honore et al., 2010). Though not statistically significant, we observed *Pitx2* induction in dual inhibition (Xav+SB; Figure S3E) cultures. Nevertheless, owing to lack of specific markers, premandibular mesoderm identity upon dual inhibition could not be ascertained. Consistent with the upregulation of *Sox2* RNA (Figure S3C), immunofluorescence assay shows Sox2+ neural clusters negative for Tbx1. Nearly 20% of the spheres in Xav+SB cultures had a few small clusters positive for Sox1+ (another neural marker; not shown). Pax3 protein was undetectable in these cultures (not shown). Mean values from 3 biological replicates plotted; error bars are SEM; p value calculated by Student's t test, unpaired; * < 0.05; Scale bar 50 μm.

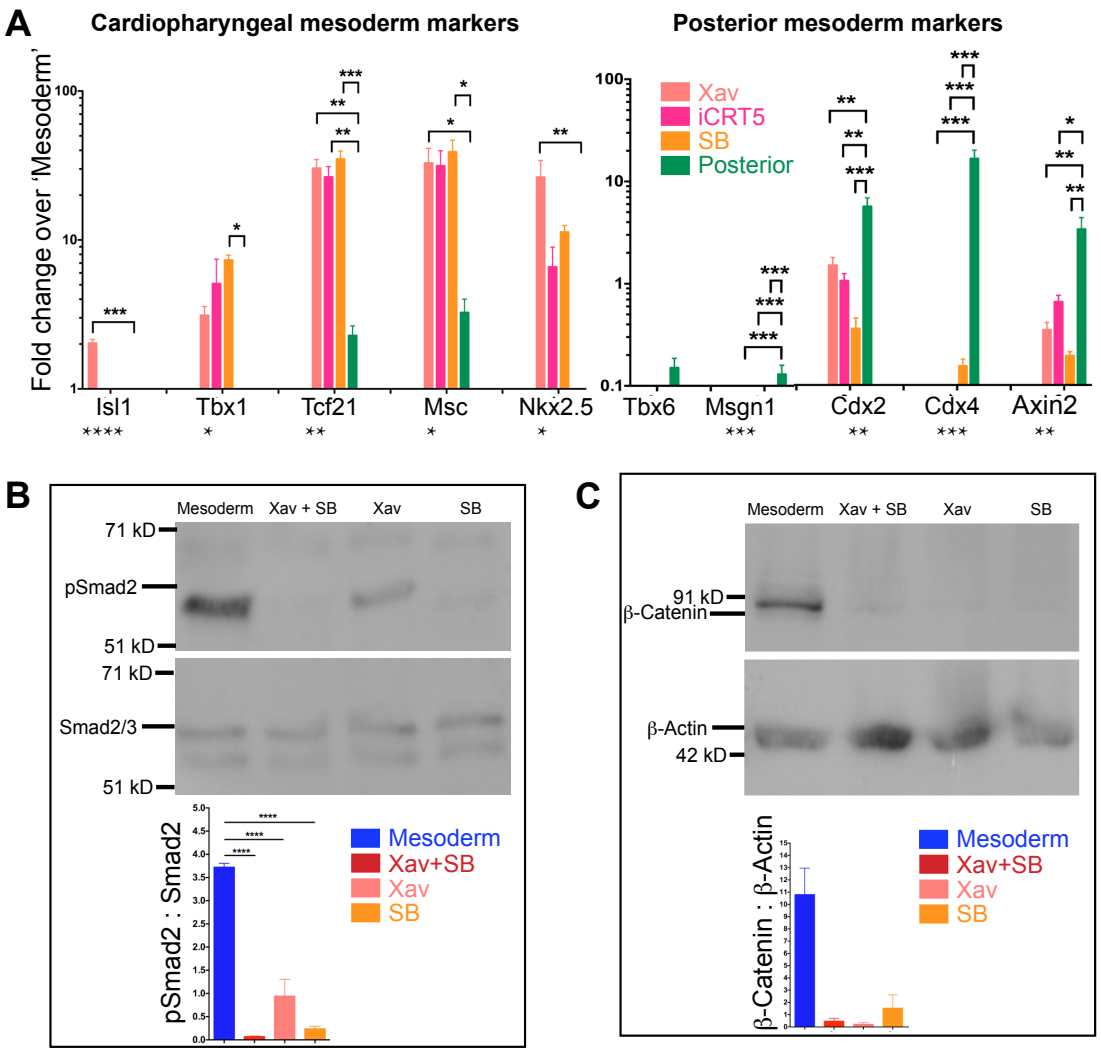

Figure S4: Cardiopharyngeal mesoderm marker induction in mESC-derived mesoderm by inhibition of Wnt and/or Nodal.

A) RT-qPCR analysis for marker genes comparing treatments with Wnt antagonist Xav 939 alone (Xav), Wnt/**β**-catenin transcription response inhibitor iCRT5 alone, Nodal inhibitor SB alone and 'Posterior'. Mean values from 3 biological replicates have been plotted; error bars are SEM; p value calculated by One-way ANOVA is indicated below X-axis. Dunnett's post hoc test was performed by pairwise comparison of individual inhibitor treatment to 'Posterior'. The significance in p value by ANOVA is indicated below X-axis and that of Dunnett's above the bars. * < 0.05, ** <0.01, *** <0.001 and so on.

B) Immunoblot shows reduced phospho-Smad 2 (p-smad2) levels verifying diminished Nodal signaling upon treatment with Xav+SB, Xav alone and SB alone. Molecular weight marker positions are indicated on the left. Histogram indicates levels of phospho-Smad2 normalized to total Smad2. For all histograms, mean values from biological triplicates have been plotted; error bars are SEM; p value calculated by One-way ANOVA is indicated below X-axis. Tukey's post hoc test was performed for pairwise comparisons of individual inhibitor treatments. n=3 experiments. The significance in p value by Tukey's is indicated above the bars. * < 0.05, ** <0.01, *** <0.001, **** <0.0001 and so on.

C) Immunoblot shows reduced β-catenin levels verifying diminished Wnt signaling upon treatment with Xav+SB, Xav alone and SB alone. Molecular weight marker positions are indicated on the left. Histogram indicates levels of β-catenin with respect to β-Actin. For all histograms, mean values from biological duplicates have been plotted; error bars are SEM. n=2 experiments.

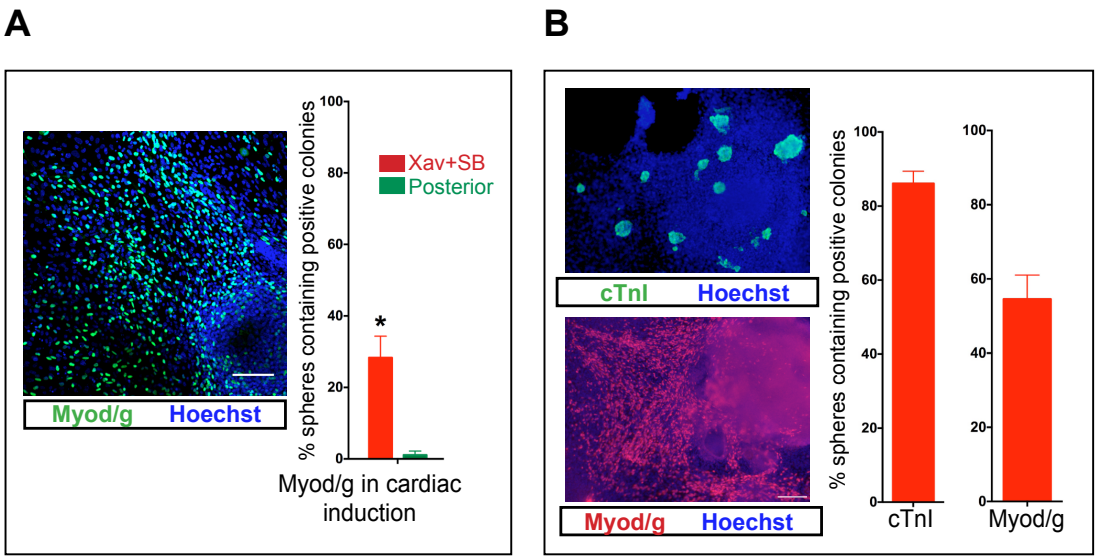

Figure S5: Dual differentiation potential of *in vitro* CPM-like population.
A) Immunostaining shows skeletal muscle differentiation in cardiogenic culture condition. Proportion of spheres associated with Myod/Myog positive clusters in cardiogenic cultures is 28.3 ± 6% (mean ± SEM) in Xav+SB-derived and 1.1 ± 1.1% in 'Posterior' derived cultures. Mean values from 3 biological replicates plotted; error bars are SEM; p value calculated by Student's t test, unpaired; * < 0.05; ** < 0.01; scale bar 100 μm.
B) Immunostaining shows skeletal and cardiac muscle differentiation from another mESC line (B6D2) when Xav+SB cells were differentiated in N2B27 containing media. Proportion of spheres associated with cardiac TroponinI positive clusters is 86.1 ± 3.3% (mean ± SEM) and proportion of spheres associated with Myod/Myog positive clusters is 54.5 ± 6.5%. Mean values from 6 biological replicates plotted; error bars are SEM; scale bar 50 μm.

Supplementary References:

Caprio, C. and Baldini, A. (2014). p53 suppression partially rescues the mutant phenotype in mouse models of DiGeorge syndrome. *Proc. Natl. Acad. Sci.* **111**, 13385–13390.

Costello, I., Pimeisl, I.-M., Dräger, S., Bikoff, E. K., Robertson, E. J. and Arnold, S. J. (2011). The T-box transcription factor Eomesodermin acts upstream of Mesp1 to specify cardiac mesoderm during mouse gastrulation. *Nat. Cell Biol.* **13**, 1084–1091.

Hadjantonakis, A. K., Pisano, E. and Papaioannou, V. E. (2008). Tbx6 regulates left/right patterning in mouse embryos through effects on nodal cilia and perinodal signaling. *PLoS One* **3**, e2511.

Harel, I., Maezawa, Y., Avraham, R., Rinon, A., Ma, H.-Y., Cross, J. W., Leviatan, N., Hegesh, J., Roy, A., Jacob-Hirsch, J., et al. (2012). Pharyngeal mesoderm regulatory network controls cardiac and head muscle morphogenesis. *Proc. Natl. Acad. Sci.* **109**, 18839–18844.

Iwafuchi-Doi, M., Matsuda, K., Murakami, K., Niwa, H., Tesar, P. J., Aruga, J., Matsuo, I. and Kondoh, H. (2012). Transcriptional regulatory networks in epiblast cells and during anterior neural plate development as modeled in epiblast stem cells. *Development* **139**, 4675–4675.

Javali, A., Misra, A., Leonavicius, K., Acharyya, D., Vyas, B. and Sambasivan, R. (2017). Co-expression of Tbx6 and Sox2 identifies a novel transient neuromesoderm progenitor cell state. *Development* **144**, 4522–4529.

Jho, E., Zhang, T., Domon, C., Joo, C., Freund, J. and Costantini, F. (2002). Wnt / β -Catenin / Tcf Signaling Induces the Transcription of Axin2 , a Negative Regulator of the Signaling Pathway Wnt / ß-Catenin / Tcf Signaling Induces the Transcription of Axin2 , a Negative Regulator of the Signaling Pathway. *Mol. Cell. Biol.* **22**, 1172–1183.

Kokkinopoulos, I., Ishida, H., Saba, R., Coppen, S., Suzuki, K. and Yashiro, K. (2016). Cardiomyocyte Differentiation From Mouse Embryonic Stem Cells Using a Simple and Defined Protocol. *Dev Dyn* 157–165.

Kurek, D., Neagu, A., Tastemel, M., Tüysüz, N., Lehmann, J., Van De Werken, H. J. G., Philipsen, S., Van Der Linden, R., Maas, A., Van Ijcken, W. F. J., et al. (2015). Endogenous WNT signals mediate BMP-induced and spontaneous differentiation of epiblast stem cells and human embryonic stem cells. *Stem Cell Reports* **4**, 114–128.

L'Honore, A., Ouimette, J. F., Lavertu-Jolin, M. and Drouin, J. (2010). Pitx2 defines alternate pathways acting through MyoD during limb and somitic myogenesis. *Development* **137**, 3847–3856.

Lolas, M., Valenzuela, P. D. T., Tjian, R. and Liu, Z. (2014). Charting Brachyury-mediated developmental pathways during early mouse embryogenesis. *Proc. Natl. Acad. Sci. U. S. A.* **111**, 4478–83.

Mendjan, S., Mascetti, V. L., Ortmann, D., Ortiz, M., Karjosukarso, D. W., Ng, Y., Moreau, T. and Pedersen, R. A. (2014). NANOG and CDX2 Pattern Distinct Subtypes of Human Mesoderm during Exit from Pluripotency. *Cell Stem Cell* 1–16.

Muzumdar, M. D., Tasic, B., Miyamichi, K., Li, L. and Luo, L. (2007). A global double-fluorescent Cre reporter mouse. *Genesis* **45**, 593–605.

Rayon, T., Menchero, S., Nieto, A., Xenopoulos, P., Crespo, M., Cockburn, K., Cañon, S., Sasaki, H., Hadjantonakis, A. K., de la Pompa, J. L., et al. (2014). Notch and Hippo Converge on Cdx2 to Specify the Trophectoderm Lineage in the Mouse Blastocyst. *Dev. Cell* **30**, 410–422.

Saga, Y., Miyagawa-Tomita, S., Takagi, a, Kitajima, S., Miyazaki, J. I. and Inoue, T. (1999). MesP1 is expressed in the heart precursor cells and required for the formation of a single heart tube. *Development* **126**, 3437–47.

Sambasivan, R., Gayraud-Morel, B., Dumas, G., Cimper, C., Paisant, S., Kelly, R. G. and Tajbakhsh, S. (2009). Distinct regulatory cascades govern extraocular and pharyngeal arch muscle progenitor cell fates. *Dev Cell* **16**, 810–821.

Shedlovsky, A., King, T. R. and Dove, W. F. (1988). Saturation germ line mutagenesis of the murine t region including a lethal allele at the quaking locus. *Proc Natl Acad Sci U S A* **85**, 180–184.

Shelton, M., Metz, J., Liu, J., Carpenedo, R. L., Demers, S. P., Stanford, W. L. and Skerjanc, I. S. (2014). Derivation and expansion of PAX7-positive muscle progenitors from human and mouse embryonic stem cells. *Stem Cell Reports* **3**, 516–529.

Tajbakhsh, S., Rocancourt, D., Cossu, G. and Buckingham, M. (1997). Redefining the genetic hierarchies controlling skeletal myogenesis: Pax-3 and Myf-5 act upstream of MyoD. *Cell* **89**, 127–138.

Tzouanacou, E., Wegener, A., Wymeersch, F. J., Wilson, V. and Nicolas, J.-F. (2009). Redefining the progression of lineage segregations during mammalian embryogenesis by clonal analysis. *Dev. Cell* **17**, 365–76.

Vallier, L. and Pedersen, R. A. (2008). Differentiation of Human Embryonic Stem Cells in Adherent and in Chemically Defined Culture Conditions. In *Current Protocols in Stem Cell Biology*, p. 4:1D.4.1-1D.4.7.